Formation planétaire et exoplanètes
Ecole CNRS de Goutelas XXVIII (2005)
Edité par J.L. Halbwachs, D. Egret et J.M. Hameury

Plasma interactions of exoplanets with their parent stars and associated radio emissions

Philippe Zarka

LESIA, CNRS-Observatoire de Paris, Meudon, France

Abstract. The relatively high contrast between planetary and solar low frequency radio emissions suggests that the low-frequency radio range may be well adapted to the direct detection of exoplanets. We review the most significant properties of planetary radio emissions (auroral as well as satellite-induced) and show that their primary engine is the interaction of a plasma flow with an obstacle in the presence of a strong magnetic field (of the flow or of the obstacle). Scaling laws have been derived from solar system planetary radio emissions that relate the emitted radio power to the power dissipated in the various corresponding flow-obstacle interactions. We generalize these scaling laws into a "radio-magnetic" scaling law that seems to relate output radio power to the magnetic energy flux convected on the obstacle, this obstacle being magnetized or unmagnetized. Extrapolating this scaling law to the case of exoplanets, we find that hot Jupiters may produce very intense radio emissions due to either magnetospheric interaction with a strong stellar wind or to unipolar interaction between the planet and a magnetic star (or strongly magnetized regions of the stellar surface). In the former case, similar to the magnetosphere-solar wind interactions in our solar system or to the Ganymede-Jupiter interaction, a hecto-decameter emission is expected in the vicinity of the planet with an intensity possibly 10^3 to 10^5 times that of Jupiter's low frequency radio emissions. In the latter case, which is a giant analogous of the Io-Jupiter system, emission in the decameter-to-meter wavelength range near the footprints of the star's magnetic field lines interacting with the planet may reach 10^6 times that of Jupiter (unless some "saturation" mechanism occurs). The system of HD 179949, where a hot spot has been tentatively detected in visible light near the sub-planetary point, is discussed in some details. Radio detectability is addressed with present and future low-frequency radiotelescopes. Ongoing searches and their preliminary results are summarized and commented. Finally, we discuss the interests of direct radio detection, among which access to ex-

oplanetary magnetic field measurements and comparative magnetospheric physics.

Contents

1. Motivation

The main limitation to the direct detection of exoplanets in the infrared or visible range is the very high contrast between the star's and the planet's luminosity, together with their small angular separation as measured from stellar distances : 1 Astronomical Unit (AU) at 1 parsec (pc) corresponds by definition to a separation of 1". In the visible range, the stellar luminosity L_* is due to the bulk of its thermal emission, whereas the planet's luminosity is simply the fraction of the star's light reflected by the planet (of the order of $L_* A \pi R_{\rm P}^2/(4\pi D^2)$ with A and $R_{\rm P}$ the planetary albedo and radius, and D the average star-planet distance). The star-planet contrast is 10^9 in this case. In the infrared, the luminosity of both the star and the planet are dominated by their thermal emission. A star being typically 50 times hotter than a giant planet and its projected area on the sky being ~ 100 times larger, the resulting contrast is of the order of 10^6 in that range.

However, in the low-frequency (LF) radio range, emissions of all magnetized solar system planets (Earth, Jupiter, Saturn, Uranus and Neptune) are less than 1-2 orders of magnitude below typical solar emissions (Figure 1). The highest contrast in favour of the planet is reached in the decameter range, where Jupiter's emissions are approximately as intense as Solar radio bursts, thus a star-planet contrast ~ 1 (Zarka et al., 1997; Zarka, 2004a). This results from the fact that, at long wavelengths, radio emissions are produced by nonthermal processes. The most efficient radio generation processes in the solar corona are related to beams of relativistic electrons propagating through the corona and producing the so-called type III bursts, plasma emission at the local plasma frequency $f_{\rm pe}$ ($f_{\rm pe} = \frac{1}{2\pi}\sqrt{\frac{N_{\rm e} e^2}{\varepsilon_0 m_{\rm e}}} \sim 9\sqrt{N_{\rm e}}$ with $f_{\rm pe}$ in kHz and $N_{\rm e}$ in cm^{-3}) or its second harmonic $2 \times f_{\rm pe}$ (Dulk, 2000; Cairns, 2004 and references therein). Planetary - especially auroral - radio emissions are produced coherently near the local cyclotron frequency $f_{\rm ce}$ ($f_{\rm ce} = \frac{eB}{2\pi m_{\rm e}} = 2.8B$ with $f_{\rm ce}$ in MHz and B in G) with an efficiency far higher than solar bursts (Zarka, 1998, 2000 and references therein).

It is thus quite natural to attempt to detect directly exoplanetary radio emissions similar to Jupiter's decameter emission using present or near-future large LF radiotelescopes. But, because LF radio observations also suffer strong limitations (strong galactic background luminosity, ionospheric perturbations, and intense natural and man-made radio frequency interference - or RFI), present instruments are generally limited to the detection of stellar radio bursts several orders of magnitude more intense than solar ones (see e.g. Güdel, 2002). Detection of Jupiter-like decameter emission is thus far from granted, as will be discussed in details in section 6. So we first summarize (section 2) our knowledge

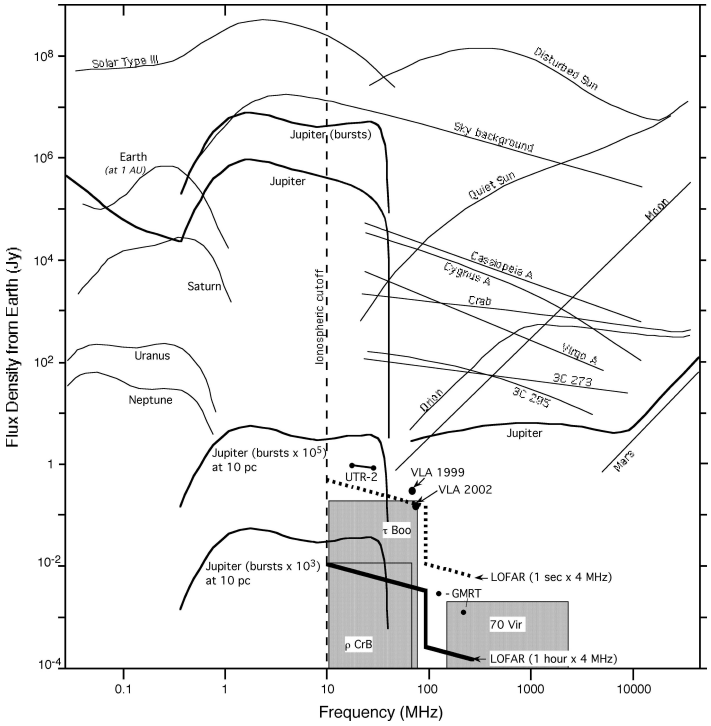

Figure 1.: *Spectra of astronomical radiosources detected from the Earth's vicinity (1 Jansky = 1 Jy =*10^{-26} *$Wm^{-2}Hz^{-1}$). Galactic, extragalactic and solar spectra are adapted from Kraus (1986). Planetary spectra, corresponding to auroral radio emissions, are adapted from Zarka (1992). Jupiter's spectrum, which includes auroral and Io-induced decameter emissions, is from Zarka et al. (2004). Its average flux density is about* 10^6 *Jy, while peak flux densities reach or exceed* 10^7 *Jy during short-lived bursts. If all planetary emissions were normalized to the same observer distance of 1 AU, Jupiter's spectrum should be upscaled by* $\times 20$*, Saturn's by* $\times 100$*, Uranus' by* $\times 400$*, and Neptune's by* $\times 900$*, so that all are grouped within 2-3 orders of magnitude of each other. Jupiter's peak spectrum is reproduced with two different scalings to illustrate the possible radio spectrum of hot Jupiters (see text). Shaded boxes are predictions from Farrell et al. (1999). Sensitivities of UTR-2, VLA, GMRT and future LOFAR observations are indicated. The Earth's ionospheric cutoff is indicated at 10 MHz.*

of planetary LF radio emissions, from the point of view of available observations as well as of their generation theory. In section 3, we focus on the primary engines of these emissions, which appear to involve in all cases the interaction of a plasma flow with an obstacle in the presence of a strong magnetic field (that of the obstacle and/or of the flow), and we estimate the corresponding dissipated powers. In section 4, we present the scaling laws derived in our solar system for relating the dissipated power at the obstacle with the emitted radio power, and we derive a "generalized Radio-Magnetic Bode's law" relating the output radio power of a magnetized flow-obstacle system to the electromagnetic Poynting flux (equivalent to the magnetic energy flux) convected on the obstacle. In section 5, we extrapolate this scaling law to the presently known exoplanets, especially the so-called "hot Jupiters", and we derive predictions for their LF radio luminosity. We also comment on the first observation interpreted as a star-exoplanet "plasma" interaction (in the system of HD 179949). Section 6 compares our predictions to the sensitivity of LF radio observations in order to assess the present and near-future detectability of radio-exoplanets. It also briefly summarizes ongoing searches, discusses their - negative - results to date, as well as expected sensitivity improvements. Finally, interest of the direct radio detection of exoplanets is recalled.

2. Planetary Magnetospheric Radio Emissions

Figure 1 displays the spectra of various radiosources that can be detected from the Earth or its vicinity. These include the sky or galactic background, various discrete sources (galaxies, nebulae, supernova remnants), solar radio emissions, and planetary radio emissions. The latter are thermal at high frequencies, nonthermal and quite intense at low frequencies.

Jupiter's radio spectrum, which extends from a few kHz to tens of GHz, is a perfect illustration of all the emission processes at work in the vicinity of a magnetized planet (Zarka, 2000). The high frequency radio spectrum, varying as f^2, corresponds to the thermal emission of the atmosphere. Between $\sim$ 100 MHz and a few GHz, synchrotron radiation more intense than thermal is produced by electrons with energies of several MeV trapped in the planetary radiation belts. Below 40 MHz, the spectrum raises by 5 orders of magnitude, and corresponds to magnetospheric radio emissions produced by a very efficient nonthermal coherent mechanism. We focus here on these latter emissions. Note that the Earth's ionosphere reflects out radio waves with frequency lower than $\sim$ 10 MHz, so that the only magnetospheric radio emission detectable from the ground is the Jovian one.

Intense radio emissions from magnetized planets were discovered in 1955 with the first observation of Jupiter's decameter bursts at 22.2 MHz, followed in the 1960's by the observation from space of the auroral kilometric radiation from the Earth itself, unable to cross the ionosphere and reach the ground because of its low frequency. Then in the 1980's the Voyager missions revealed similar kilometric radio emissions produced near the magnetic poles of Saturn, Uranus and Neptune. The common properties shared by these radio emissions are (see e.g. Zarka, 1998):

- high intensities (brightness temperatures $T_b > 10^{15-20}$ K) and consequently large emitted powers (average between 10^6 W for Neptune and 10^{11} W for Jupiter);
- instantaneous emission at the local electron cyclotron frequency $f \sim f_{ce}(\mathbf{s})$ (with $\mathbf{s}$ the location along the source field lines) and broad overall bandwidth ($\Delta f \sim f$);
- sources distributed along high latitude magnetic field lines, where energetic (a few keV) electrons precipitate; these sources are depleted and strongly magnetized ($f_{pe} \ll f_{ce}$);
- 100% circular of elliptical polarization, consistent with extraordinary (X) magneto-ionic mode;
- very anisotropic beaming of the radio emission ($\Omega \ll 4\pi$), at large angle from the magnetic field in the source, causing the deep modulation of the emission by the planetary rotation; modulations by solar wind (SW) fluctuations are also observed;
- some components are strongly modulated by the phase of a satellite (Io and Ganymede at Jupiter) as seen from the observer;
- emissions include slowly varying components (which last minutes to hours), as well as bursts ($\leq$1 sec) as shown in Figure 2.

The theoretical generation mechanism consistent with these constraints is the cyclotron-Maser instability (CMI) which builds up on unstable keV electron populations in regions where $f_{pe} \ll f_{ce}$. It can directly convert $\geq$1% of the total electron (perpendicular) energy into coherent cyclotron X-mode waves (Louarn, 1992; Zarka, 1998, 2004b and references therein).

The planetary radiosource regions that fulfill the CMI requirements are the high latitude field lines connected to various electrodynamic "engines" accelerating charged particles to several keV. These include (i) magnetic reconnection between planetary and SW magnetic field lines at

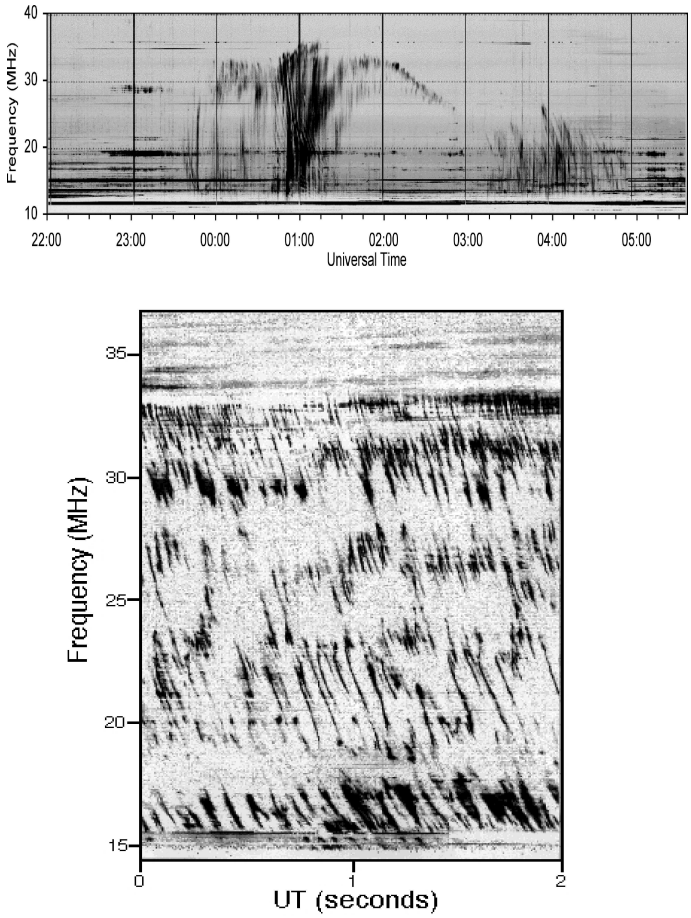

Figure 2.: *(top) Dynamic spectrum of a typical Io-Jupiter emission recorded on 1/1/1991 at the Nançay Decameter Array (NDA), in right-hand circular polarization, with time resolution* ~ 1 *sec/spectrum. Horizontal lines are man-made interference, vertical lines are calibrations. (bottom) High resolution dynamic spectrum of Jovian short bursts recorded at NDA using an acousto-optical spectrograph, with resolution of 3 msec/spectrum.*

the magnetopause nose (see Cowley et al., 2004, for Saturn), (ii) magnetic reconnection following magnetotail field pinching (Dungey, 1961), (iii) magnetospheric plasma corotation breakdown (see Cowley and Bunce, 2001, for Jupiter), (iv) magnetopause surface waves (see Galopeau et al., 1995, at Saturn), or (v) interaction between conducting satellites and the planetary magnetic field (Saur et al., 2004). These engines produce bright polar UV auroras at northern and southern magnetic field line footprints in the atmosphere and associated radio emissions above them (Prangé and Zarka, 2003; Clarke et al., 2004). The latter engine corresponds to the Io-Jupiter or Ganymede-Jupiter radio emissions and associated atmospheric UV spots (Prangé et al., 1996; Zarka, 2004c), as shown in Figure 3.

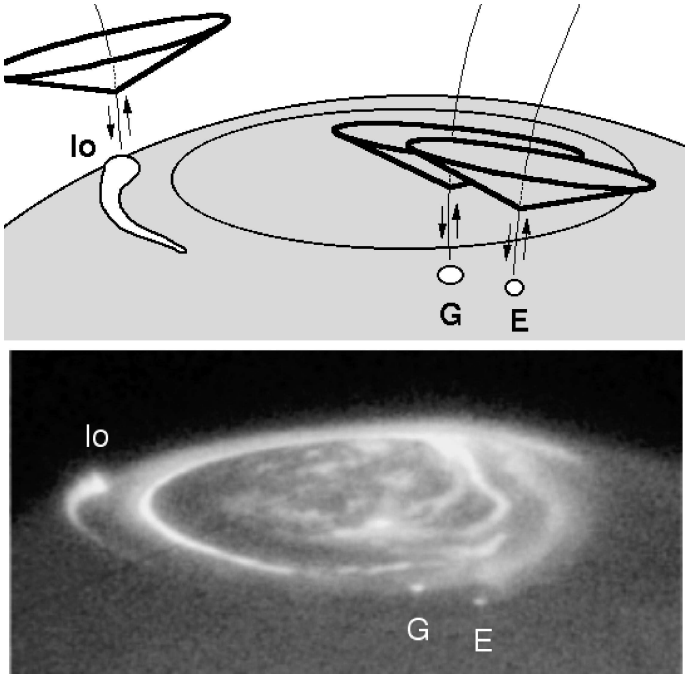

Figure 3.: *(bottom) HST UV image of northern Jovian auroral regions, showing clearly the bright main auroral oval and the footprints of Io (plus a tail-like structure), Ganymede and Europa flux tubes (courtesy R. Prangé, L. Pallier, and J.T. Clarke). (top) sketch of radio emission hollow conical beams produced above the UV hot spots by the energetic electrons precipitated along the satellite flux tubes or reflected upwards by magnetic mirroring. Similar radio emission originates from sources distributed above the main oval.*

Radio emissions with highest frequencies are produced just above the ionosphere, and increasingly lower frequencies are emitted at increasing distances up to a few planetary radii. The Earth, Saturn, Uranus and Neptune all have surface fields between 0.1 and 1 G (Encrenaz et al., 2004), and emit thus auroral radio waves with frequencies < 1-2 MHz, not detectable from the ground (Figure 1). Only Jupiter, with a surface field up to 14 G, produces emissions up to 40 MHz. The 5 "radio" planets give birth together to at least 7 radio components (5 auroral + 2 satellite-driven), each split in two sub-components (one per magnetic hemisphere).

As mentioned above, a strong correlation is observed between SW fluctuations (density, velocity and/or ram pressure) and auroral radio outputs of the Earth (Gallagher and d'Angelo, 1979), Saturn (Desch, 1982), and Jupiter (Genova et al., 1987). This correlation may originate from magnetic reconnection in the tail or at the magnetopause nose (Farrell et al., 1999), or from the magnetospheric response to compressions by the solar wind (Prangé et al., 2004).

3. Primary Engines

The strong SW control exerted on auroral radio emissions suggests that the SW-magnetosphere interaction is an important driver of the emissions. This interaction can be decomposed into (i) the dissipation of SW kinetic flow power on the magnetospheric cross-section :

$$P_{\rm flow} \sim NmV^3\pi(fR_{\rm MP})^2 \tag{1}$$

with $N = N_0/d^2$ the SW number density (N_0 being the density at Earth orbit and d the distance to the Sun in AU), V its velocity, $m \sim 1.1 \times m_{\rm p}$, $R_{\rm MP}$ the subsolar magnetopause radius and f its flaring factor (typically 1. to 1.5; see e.g. Belenkaya et al., 2005 - we will omit it for simplicity in the following); and (ii) the interplanetary magnetic field (IMF) Poynting flux on the magnetospheric cross-section:

$$P_{\rm IMF} = \int_{MP} (\mathbf{E} \times \mathbf{B}/\mu_{\mathbf{0}}).\mathbf{dS} \tag{2}$$

As $\mathbf{E} = -\mathbf{V} \times \mathbf{B}$, one finds that the radial component of $\mathbf{E} \times \mathbf{B}$ is equal to $V{B_\perp}^2$, thus

$$P_{\rm IMF} = \frac{V{B_\perp}^2}{\mu_0}\pi{R_{\rm MP}}^2 \tag{3}$$

with $B_\perp$ the IMF component perpendicular to the SW flow in the planet's frame. The magnetopause radius is fixed by the pressure equilibrium between the planetary magnetic field and the SW ram pressure:

$$R_{\rm MP} = R_{\rm P} \times \left(\frac{2B_{\rm P}^2}{K\mu_0 N m V^2} \right)^{1/6} \quad (4)$$

with $R_{\rm P}$ the planetary radius, $B_{\rm P}$ the planet's equatorial surface field, K = 1–2 depending on details of SW particle reflection at the magnetopause, and N, m, V characterizing the solar wind. Part of the dissipated energy is involved in acceleration of electrons to several keV. These electrons will follow planetary field lines to reach strongly magnetized regions where $f_{\rm pe} \ll f_{\rm ce}$. There, intense radio emissions can be produced via the CMI.

In the solar wind, beyond $\sim$ 1 AU from the Sun, the kinetic flow power is $\sim$ 170 times larger than the IMF Poynting flux. This ratio remains constant until very far from the Sun : V and m are essentially constant while N varies in $1/d^2$ (due to mass conservation during expansion), thus the kinetic flow power per unit area $\sim NmV^3$ also varies in $1/d^2$; conversely, the radial IMF component B_r varies in $1/d^2$ (due to magnetic flux conservation), and the azimuthal field along the Parker spiral $B_\varphi = B_r \times \Omega d/V$ varies thus in $1/d$ (with $\Omega = 2\pi/P_{\rm S}$ the solar rotation circular frequency; $P_{\rm S} \sim$ 27 days) (see e.g. Behannon, 1978). Beyond 1 AU, $B_\varphi > B_r$ (the ratio B_φ/B_r is about 1 at the Earth's orbit, 5 at Jupiter's orbit, and 10 at Saturn's orbit), so that $B_\perp \sim B_\varphi$, and the IMF Poynting flux per unit area $\sim V{B_\perp}^2/\mu_0$ also varies in $1/d^2$. The SW interaction with a planetary magnetosphere corresponds thus to the interaction of a weakly magnetized plasma flow with a strongly magnetized obstacle.

Alternate flow-obstacle configurations involve a strong magnetic field and also lead to intense radio emission generation (see Table 1). Those correspond to the case of a strongly magnetized plasma flow interacting with a strongly or weakly magnetized (or even unmagnetized) obstacle (rightmost column of Table 1). Both cases do exist in the interaction of the Jovian magnetosphere with the galilean satellites. Due to the strong magnetic field intensity and low plasma density in the Jovian magnetosphere (e.g. Neubauer, 1998), the magnetic energy ($\sim B^2/\mu_0$) convected onto/past a galilean satellite is much larger than the kinetic energy ($\sim NmV^2$) of the magnetospheric (corotating) plasma flow, a situation opposite to the SW-magnetosphere case. At Io, for example, the Jovian magnetic field is perpendicular to the magnetospheric plasma flow and its amplitude is $B \sim$0.02 G, the relative velocity between the corotating magnetospheric field and plasma Io's orbital motion is $V \sim$57 km/s, and the maximum plasma number density reaches $N \sim$2000 cm^{-3} in the Io torus, with a typical molecular mass $m \sim 20 \times m_{\rm p}$. The corresponding ratio $(B^2/\mu_0)/(NmV^2)$ is about 15.

Table 1.: *The various types of plasma flow – obstacle interactions. Examples are given in italics. Intense CMI–driven radio emissions can be produced in 3 cases (underlined) out of 4.*

Obstacle \ Flow	Weakly/Not magnetized *(Solar wind)*	Strongly magnetized *(Jovian magnetosphere, Stellar wind of magnetic star)*
Weakly/Not magnetized *(Venus, Mars, Io, Unmagnetized hot Jupiters ?)*	No Intense Cyclotron radio emission	Unipolar interaction → Io–induced radio emission, *Unmagnetized hot Jupiters ?*
Strongly magnetized *(Earth, Jupiter, Saturn, Uranus, Neptune, Ganymede, Magnetized hot Jupiters ?)*	Magnetospheric Interaction → Auroral radio emissions: E, J, S, U, N, *Magnetized hot Jupiters ?*	Dipolar interaction → Ganymede–induced radio emission, *Star–Planet magnetic reconnection ?*

When the satellite is magnetized, as is the case for Ganymede, it develops its own magnetosphere, embedded in that of Jupiter. Interaction between the satellite and the Jovian magnetic field is believed to happen primarily through continuous reconnection of the satellite's and the planet's magnetic field (Kivelson et al., 1997a) (Figure 4). Such an interaction will be qualified of "dipolar" hereafter. Note that the radius of Ganymede's magnetopause is about 2.5 to 3 times the radius of the moon itself (Gurnett et al., 1996; Kivelson et al., 1996, 2004).

When the satellite is weakly magnetized or unmagnetized, as is the case for Io or Europa, its ionosphere (and induced field) interacts with the Jovian field through MHD waves (Alfvén waves, slow mode waves or slow mode shocks) generating "wings" across the jovian field downstream of the satellite (Neubauer, 1980 ; Erkaev et al., 2002; Kivelson et al., 2004; Saur et al., 2004) (Figure 5). Such an interaction will be qualified of "unipolar", although strictly speaking the "unipolar inductor" case corresponds to very large Alfvén velocities between the satellite and the planet and thus quasi–instantaneous setup of a field–aligned current circuit (Goldreich and Lynden–Bell, 1969). When the satellite–planet Alfvén travel time is longer that the convection time of the magnetospheric field and plasma past the satellite, "wings" are generated

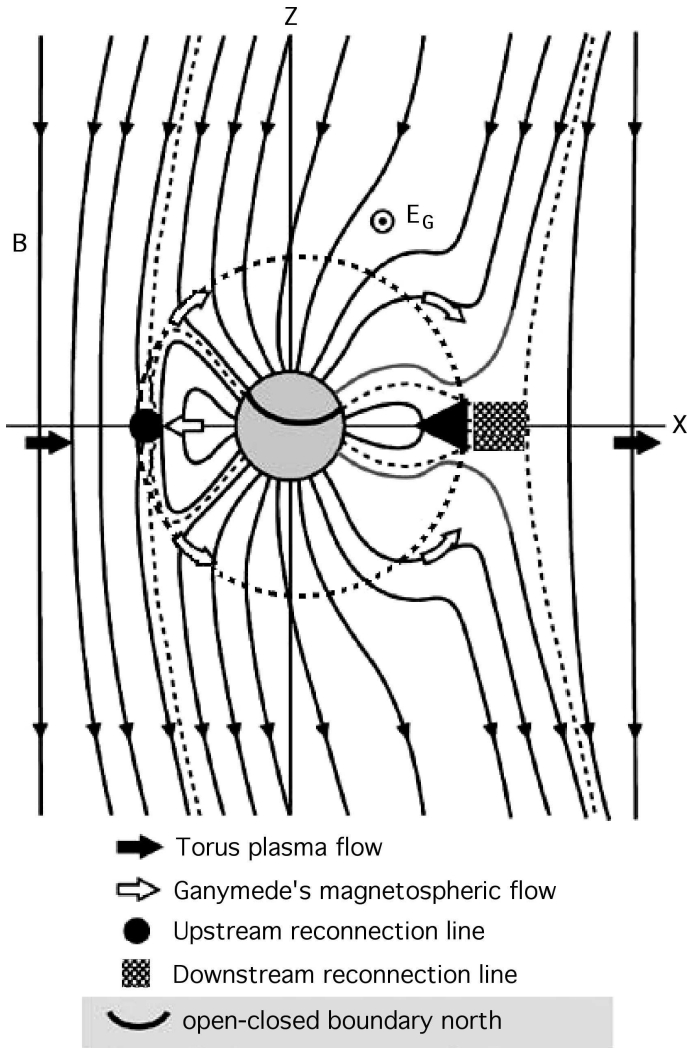

Figure 4.: *Fields and flows in the vicinity of Ganymede. The Y axis points towards Jupiter. The extent of Ganymede's magnetosphere (i.e. Ganymede–dominated field region) is represented as the dotted sphere of radius* $\sim$*2.5* R_G *(adapted from Kivelson et al., 2004).*

as the envelope of the perturbation traveling from the satellite to the planet in both hemispheres. In that case, the high latitude signatures of the satellite–magnetosphere interaction (see section 2 and Figure 3) are shifted from the instantaneous satellite longitude, leading it by an angle $\delta = 2\pi t_{\rm A}/P_{\rm syn}$ (with $t_{\rm A}$ the Alfvén travel time and $P_{\rm syn}$ the planetary rotation period as seen from the satellite – see Figure 6 of Zarka, 2004c). $\delta = 3^\circ - 20^\circ$ in the Io–Jupiter case. This angle is modified by the planetary magnetic field topology because field lines are not necessarily contained in a meridian plane. Based on available Jovian internal field models (Connerney, 1992; Connerney et al., 1998), the longitude of the instantaneous Io field line footprint may differ by $\pm 40^\circ$ from that of Io. For such an interaction between an unmagnetized satellite and the Jovian field, the radius of the obstacle to be considered is the typical exo–ionospheric radius, taken as $1.1\times$ to $1.4\times R_{\rm Io}$ in the case of Io (Kivelson et al., 1997b).

The power dissipated through the "dipolar" interaction ($P_{\rm d}$) can be estimated from the reconnected magnetic flux at the magnetopause. Following Akasofu (1981, 1982) we can express the flow–magnetosphere reconnected power as the Poynting flux on the magnetopause cross–section, or equivalently (following equation 2):

$$P_{\rm d} = \frac{\varepsilon K V B_\perp^2}{\mu_0} \pi {R_{\rm MP}}^2 \tag{5}$$

with ε a reconnection efficiency of the order of 0.1–0.2, and K a function that "triggers" the reconnection in response to the magnetosphere state (open or closed). Depending on the orientation of the planetary dipole field, K is represented by a $\sin^4(\theta/2)$ (for Earth) or $\cos^4(\theta/2)$ function (for Jupiter and Saturn), θ being the angle between the magnetic field embedded in the flow and the field of the obstacle. The relative orientation of Ganymede's field and of the Jovian field is such that $K \sim 1$ (open magnetosphere case). Thus, the dissipated (reconnected) power may be written:

$$P_{\rm d} \sim \frac{\varepsilon V B_\perp^2}{\mu_0} \pi {R_{\rm MP}}^2 \tag{6}$$

It is a fraction ε of the incident Poynting flux ($VB_\perp^2/\mu_0$ on the obstacle of cross–section ($\pi R_{\rm MP}^2$, with $R_{\rm MP} \sim 2.5 - 3 \times R_{\rm G}$ the radius of Ganymede's magnetosphere). The strongly magnetized environment of Ganymede leads to expect a value of ε larger than in the Earth's magnetosphere case, up to 0.3 (Kivelson et al., 1997a). Ip et al. (2004) have studied via MHD simulations the shape of magnetospheric (obstacle) field

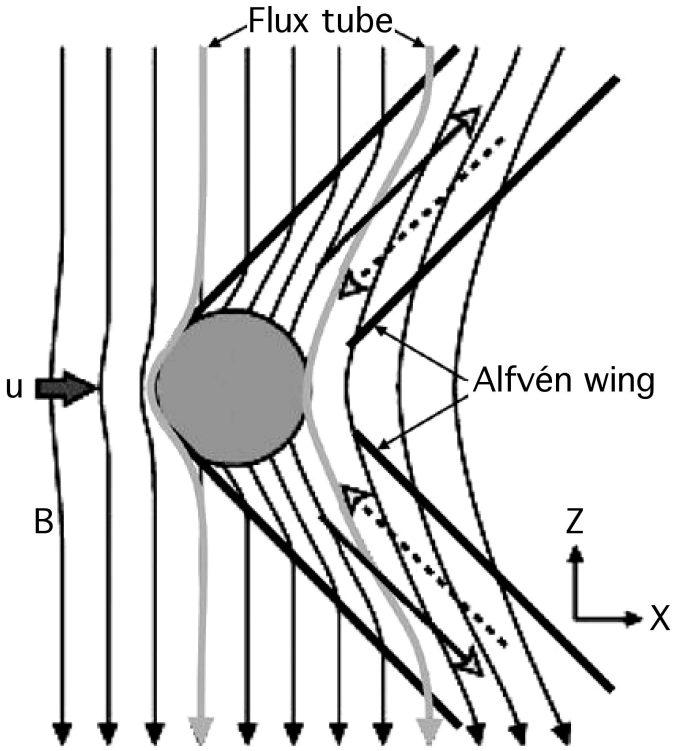

Figure 5.: *Sketch of Io's Alfvén wing across Jupiter's magnetic field (B, southward).* $\boldsymbol{u}$ *represents the incident flow velocity. The Y axis points towards Jupiter. Solid (resp. dashed) arrows –with open heads– represent currents flowing on the anti–Jupiter (resp. on the Jupiter) side of the IFT. (adapted from Kivelson et al., 2004).*

lines as a function of the orientation of the magnetic field embedded in the plasma flow.

In the case of the Io–Jupiter "unipolar" interaction, the dissipated power has been estimated via several mutually consistent approaches. The potential drop across the obstacle (Io's ionosphere) is:

$$\phi = E \times 2R_{\rm obs} = V \times B_{\perp} \times 2R_{\rm obs} \tag{7}$$

with V =57 km/s, $B_{\perp} = B_{\rm J}$ the Jovian field at Io's orbit ($\sim$ 0.02 G), thus $E \sim 0.1$ V/m, and an obstacle radius $R_{\rm obs} = (1.1 - 1.4) \times R_{\rm Io}$, thus $\phi \sim 500$ kV. The Voyager 1 spacecraft deduced from magnetic field perturbations measured near Io that a current of intensity $I = 2-3\times10^6$ Amperes was circulating in the Io flux tube (IFT), thus a first crude estimate of the dissipated power is:

$$P_{\rm d} = I \times \phi \sim 10^{12}{\rm W\ (per\ hemisphere)}$$

A nonlinear MHD analysis of the Io–Jupiter circuit led Neubauer (1980) to infer the existence of currents perpendicular to the Jovian magnetic field in the Alfvén wings, contributing to close the Io current circuit (instead of Jupiter's ionosphere only in the unipolar inductor case of Goldreich and Lynden–Bell 1969). Neubauer (1980) expressed the Alfvén conductance as:

$$\Sigma_{\rm A} = \frac{M_{\rm A}}{\mu_0 V \sqrt{1 + M_{\rm A}^2}}$$

when the flow is strictly perpendicular to the field ($M_{\rm A} = V/V_{\rm A}$ is the Alfvén Mach number, with $V_{\rm A} \sim B/\sqrt{Nm\mu_0}$), and derived a dissipated power:

$$P_{\rm d} = \Sigma_{\rm A} \times E^2 \times \pi R_{\rm obs}^2 \sim 10^{12}{\rm W\ (per\ hemisphere)}$$

Following Zarka et al. (2001a), we rewrite the above expression as:

$$P_{\rm d} = (1 + M_{\rm A}^{-2})^{-1/2} \frac{V B_{\perp}^2}{\mu_0} \pi {R_{\rm obs}}^2 \tag{8}$$

This expression is identical to (5) except for the factor $(1+M_{\rm A}^{-2})^{-1/2}$ instead of ε. Whatever the value of $M_{\rm A}$, one has

$$M_{\rm A} \leq (1 + M_{\rm A}^{-2})^{-1/2} \leq 1$$

The Io–Jupiter interaction occurs in sub–Alfvénic regime, with $M_{\rm A}$ =0.15 to 0.3, implying $(1 + M_{\rm A}^{-2})^{-1/2} = 0.15$ to 0.3, very similar

to the expected value for ε. The detailed values of the efficiency also depends (through E) on the conductivity of the obstacle.

We infer thus a general estimate for the power dissipated $P_{\rm d}$ via a satellite–magnetosphere interaction, be it "unipolar" or "dipolar":

$$P_{\rm d} \sim \frac{\varepsilon V B_\perp^2}{\mu_0} \pi {R_{\rm obs}}^2 \qquad (9)$$

This very general expression is simply the fraction ε of the magnetic energy flux convected on the obstacle. It is expected to provide a correct order of magnitude whatever the interaction regime (super– or sub–Alfvénic), as long as the obstacle conductivity is not vanishingly small. At Io, the obstacle is the extended exo–ionosphere, of radius (1.1–1.4) $\times R_{\rm Io}$. At Ganymede, the obstacle is the magnetopause, of radius (2.5–3.0) $\times R_{\rm G}$. At Europa and Callisto, conductivity may be provided by a subsurface ocean (Khurana et al., 1998) and/or an extended plasma cloud of density up to 100–400 cm^{-3} (Kurth et al., 2000 ; Gurnett et al., 2000). We use for these two satellites an obstacle size between 1.0 and 1.2 times their diameter.

Table 2 lists the predicted values of $P_{\rm d}$ for the 4 galilean satellites, computed with $\varepsilon = 1$ by analogy with the SW–magnetosphere case (the efficiency will be included in the "Radio–Magnetic Bode's law" – see below). It is remarkable that a similar power is dissipated at Europa and Ganymede, $\sim$10 times smaller than in Io's case. Although Ganymede is farther from the planet, hence a magnetic energy density $\sim$20 times weaker at Ganymede's orbit than at Europa's, its magnetosphere has an electrodynamic cross–section $\sim$20 times as large as Europa's conductive interior/envelope. $P_{\rm d}$ is weaker for Callisto, but also much more variable due to the crossing by Callisto of the Jovian current disk twice per Jovian rotation. The maximum value of $P_{\rm d}$ for Callisto is only 6 times weaker than the minimum dissipated power for Ganymede and Europa.

4. Scaling laws for the emitted radio power

As mentioned above for the SW–magnetosphere case, part of the energy dissipated in the flow–obstacle interaction is involved in the acceleration of electrons to keV or more. The same is true in the case of a strongly magnetized flow. Whatever the interaction type, "unipolar" or "dipolar", it should lead to field–aligned currents circulating between the obstacle (e.g. the satellite) and the source of the magnetic field (e.g. the planet). In the Jovian case, due to the low magnetospheric electron density, the necessity to sustain these currents leads to electron acceleration (Knight, 1973). Electrons precipitating towards high Jovian latitudes in/near the IFT also have an energy of several keV to tens of

Table 2.: *For each galilean satellite we list : the orbital distance in R_J (1 R_J = 71400 km) ; the (min–max) Jovian field amplitude at the satellite orbit, computed from the O6 or VIP4 internal field model with current sheet; the relative velocity V=$V_{corot} - V_{orb} = \Omega_J L R_J - \sqrt{\frac{GM_J}{LR_J}}$; the estimated obstacle size as discussed in the text ; the deduced (min–max) dissipated power following equation (9) ; the estimated radio power (see section 4) ; the estimated emitted UV power ; the qualitative interaction strength (from Kurth et al., 2000).*

Satellite	L (R_J)	B_J(G)	V(km/s)	R_{obs}(km)
Io	5.9	$(1.8-2.1)\times10^{-2}$	57	$(1.1-1.4)\times$ 1820
Europe	9.4	$(4.0-5.0)\times10^{-3}$	104	$(1.0-1.2)\times$ 1560
Ganymede	15	$(0.7-1.5)\times10^{-3}$	177	$(2.5-3.0)\times$ 2630
Callisto	26.4	$(0.5-4.7)\times10^{-4}$	323	$(1.0-1.2)\times$ 2410

Satellite	P_d (W/hem.)	P_{Radio}(W)	P_{UV} (W)	Interaction strength
Io	$(1.8-4.1)\times10^{12}$	$0.3-3\times10^{10}$	$(2-10)\times10^{10}$	Strongest
Europe	$(1.0-2.3)\times10^{11}$	?	$(1-10)\times10^{9}$	Intermediate
Ganymede	$(0.9-6.2)\times10^{11}$	$\sim10^{9}$	$(1-10)\times10^{9}$	Intermediate
Callisto	$(0.1-15.)\times10^{9}$	$\leq 8.5\times10^{8}$	?	Weakest

keV (Prangé et al., 1996; Zarka et al., 1996). In summary, in all the cases underlined in Table 1, keV electrons are produced and propagate along magnetic field lines towards the main source of the strong magnetic field (the planet in the SW–magnetosphere case, Jupiter in the case of Io and Ganymede interactions, the central magnetic star in the case of a hot Jupiter – magnetic star system as discussed below. In the vicinity of this source, plasma conditions ($f_{\rm pe} \ll f_{\rm ce}$) generally allow for the generation of intense radio emissions via the CMI. The latter microscopic generation mechanism has been extensively studied and its efficiency can be quantified from the knowledge of the plasma and field conditions in the source and from the distribution function of energetic (emitting) electrons. But, the steps leading from the overall dissipated energy (equations 1, 3 & 9) to the energy and distribution of accelerated electrons are not known quantitatively enough for allowing us to predict the emitted radio power from the dissipated power.

Fortunately, from the study of the many examples provided in our solar system, scaling laws can be derived that include the above poorly quantified steps in a macroscopic empirical "efficiency factor". In 1984 was introduced the so–called "radiometric Bode's law" (Desch and Kaiser, 1984) relating the auroral radio power emitted by Jupiter, Saturn and the Earth to the incident kinetic flow power on the magnetosphere's cross section (given by equation (1)). Zarka (1992, 1998) extended this law to the auroral radio emissions from Uranus and Neptune. In order not to mix auroral emissions resulting from the SW–magnetosphere interaction with similar emissions resulting from internal magnetospheric processes (as the Io–Jupiter interaction), Desch and Kaiser (1984) restricted the Jovian radio emission to the hectometer range (∼200 kHz to 3 MHz). Zarka (1992, 1998) included the decameter emission independent of Io. The result, shown in Figure 6, is a striking correlation between the output planetary radio power and the SW kinetic power incident on the magnetopause, valid over about 4 orders of magnitude, with fluctuations about a factor 2 of individual points around the best fit line. Moreover, the slope of this line is very close to 1, i.e. the output radio power is directly proportional to the input SW power. The "efficiency factor" is $\eta_k \sim 10^{-5}$ (with $N_0 = 5$ cm^{-3}). Noting (section 3) that beyond ∼1 AU the IMF Poynting flux per unit area ($\sim VB_\perp^2/\mu_0$) varies as the kinetic flow power per unit area ($\sim NmV^3$), i.e. in $1/d^2$, the same correlation as above exists between the planetary auroral radio power and the IMF Poynting flux onto the magnetospheric cross–section. As the SW magnetic energy density is ∼ 170 times smaller that its flow kinetic energy density, the efficiency factor for the "Radio–Magnetic Bode's law" is $\eta_{\rm m} \sim 2 \times 10^{-3}$ (Figure 6).

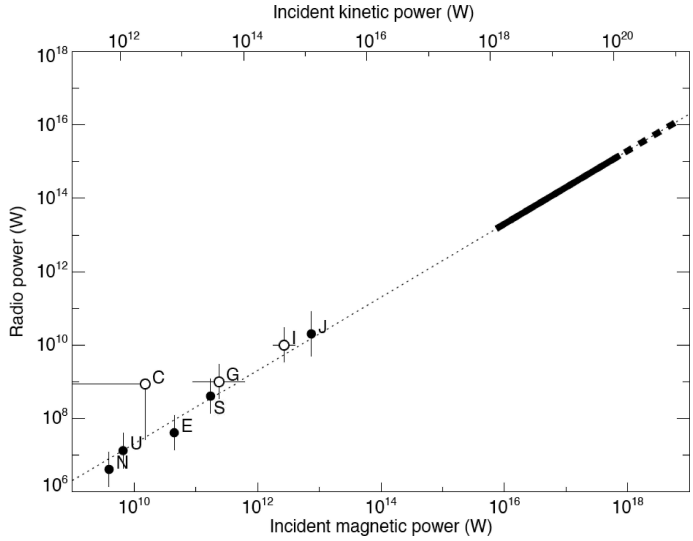

Figure 6.: *Generalized "Radio Bode's laws" showing the proportionality (slope* ~ 1*) between output planetary radio powers and the SW power (kinetic –upper horizontal scale– or magnetic –lower horizontal scale) incident on the magnetopause. E, J, S, U, N are the initials of the 5 radio planets. Kinetic–to–radio efficiency is* $\sim 10^{-5}$*, magnetic–to–radio efficiency is* $\sim 2 \times 10^{-3}$*. Open dots show the correlation between induced radio emissions from Io, Ganymede and an upper limit for Callisto, and dissipated magnetic power deduced from equation (9) and Table 2. The thick bar results from extrapolation to hot Jupiters of the SW–planet magnetospheric interaction (solid) and dipolar and unipolar star–planet interaction (dashed).*

¿From these two observed scaling laws alone, it is not possible to decide which incident power actually drives the auroral radio power. Even if the incident kinetic power largely dominates the magnetic one, their respective roles will depend on the actual efficiencies of the conversion of each power into electron acceleration. Note that Akasofu (1982) already concluded that the total energy output (or "consumption") of the Earth's magnetosphere, as defined via geomagnetic indexes, correlated best with the reconnected magnetic power expressed by equation (9) (rather than with the SW kinetic power of equation (1)).

In the case of Jupiter–satellite interactions, the energetic electrons precipitated along the satellites flux tubes or reflected upwards by magnetic mirroring near the Jovian ionosphere also produce intense nonthermal radio emissions (Figures 2 & 3). The radio output power is difficult to estimate because the absence of angular resolution of LF radio measurements implies that the satellite–induced nature of part of the observed emissions is determined on a statistical basis only. The best available estimate for the average detected power of Io–induced radio emissions, derived from integration over time, emission bandwidth and beaming pattern, is $\sim 10^{10}$ W (Kaiser et al., 2000 ; Queinnec and Zarka, 2001; Zarka et al., 2004). Instantaneous values typically span the range $0.3–3\times 10^{10}$ W, which requires $3–10 \times 10^{11}$ W precipitations in 1–10 keV electrons. Less accurate estimates are available for Europa, Ganymede, and Callisto. Menietti et al. (1998, 2001) have searched for the influence of these satellites on Jupiter's hecto–decameter emission by analyzing Galileo/PWS observations in the range 2.0–5.6 MHz. The results have been synthesized and compared to Cassini/RPWS observations by Hospodarsky et al. (2001): the occurrence and intensity of radio emissions detected by Galileo above a threshold of 4×10^{-18} W/m^{2}Hz were binned in 6° longitude × 6° satellite phase bins; increased occurrence probability and average intensity were found at specific orbital phases of Ganymede and Callisto. The average isotropic power in high intensity bins is $\sim 4\times 10^7$ W for Ganymede and Callisto, versus 5.6×10^7 W for Io (Menietti et al., 2001), but occurrence rates of induced emissions are much weaker for the former. As deduced by comparing peak amplitude to baseline level in Figure 3 of Hospodarsky et al. (2001), the occurrence probability of Io–induced emission is typically ∼1.6 times that of the satellite–independent one. For Ganymede, the occurrence probability is ∼0.16 (0.029/0.18) times that of the satellite–independent emissions, and for Callisto $\leq$0.14 times (0.025/0.18 – the latter case is very noisy). Referring to a 10^{10} W average power for the Io–induced emission, and assuming similar bandwidth and beaming patterns for all satellite–induced emissions, one gets rough estimates of 10^9 W for Ganymede and an upper limit of 8.5×10^9 W for Callisto. No Europa–induced radio emission was

found. This may be due to the 2:1 orbital resonance between Io and Europa which may "hide" weak Europa–induced radio emissions in stronger Io–induced ones. No correlation of radio emissions with satellites other than Io could be found in the limited Cassini/RPWS database.

The energetic electrons precipitated along the satellite flux tubes also produce induced aurorae in the form of bright UV spots at their atmospheric footprints due to collisionnal excitation of atmospheric species (mainly H and H_2). The intensity of these spots varies with the longitude, and corresponds in the case of Io to a radiated UV power of 2–10$\times 10^{10}$ W (in H Ly–α and H_2 Lyman and Werner bands), requiring a 1–6$\times 10^{11}$ W precipitation power under the form of 10–100 keV electrons (Prangé et al., 1996, 1998; Clarke et al., 2002). The IFT northern and southern footprints have also been detected in the infrared (H_3^+) (Connerney et al., 1993) and require a similar precipitation power. On recent HST UV images of northern Jovian auroral regions, one can see clearly the bright footprints of Ganymede's and Europa's flux tubes (Figure 3). Only a few quantitative measurements of these footprints have been published so far: Clarke et al. (2002) estimated their brightness to be one order of magnitude weaker than Io's ones (tens of kilorayleighs for Ganymede and Europa versus hundreds for Io). Taking into account the smaller spot sizes (as compared to Io's), one obtains a radiated UV power about 1–10$\times 10^9$ W for Ganymede and Europa (Clarke et al., 2002; Prangé and Zarka, 2003). No UV spot has been detected at Callisto's flux tube footprint, but this is due to the fact that it would lie directly inside the main auroral oval.

Finally, based on local plasma wave observations by Galileo, Kurth et al. (2000) have qualitatively classified the interaction strength of the 4 galilean satellites with Jupiter's magnetic field: again, Io has the strongest interaction; Europa and Ganymede are "intermediate", and Callisto has the weakest interaction. This, and the fact that 8.5×10^9 W represents an exceedingly large fraction of the available power at Callisto's orbit, further suggests that the radio powers derived above for Callisto are upper limits.

Table 2 summarizes the estimates discussed above for the energetics of satellite-Jupiter induced electromagnetic emissions. With the exception of $P_{\rm Radio}$(Callisto), comparison of the last 4 columns shows a consistent relationship between the radiated powers, interaction strength, and predicted dissipated powers. The overall radio efficiency ($P_{\rm Radio}/P_{\rm d}$) is 0.2 – 1%, and the UV efficiency ($P_{\rm UV}/P_{\rm d}$) is 1 – 5%. The former range is consistent with the above "Radio–Magnetic Bode's law" (0.2%), so that on Figure 6, the points representing the Io– and Ganymede–Jupiter interactions fall close to the best fit line. We obtain thus empirically a "generalized Radio–Magnetic Bode's law" relating the output radio

power of a magnetized flow–obstacle system to the magnetic energy flux convected on the obstacle:

$$P_{\rm Radio} \sim \eta \times P_{\rm d} \tag{10}$$

with $\eta \sim 2 - 10 \times 10^{-3}$ and $P_{\rm d}$ given by equation (9) with $\varepsilon = 1$. We propose that this scaling law represents more than a coincidence, but rather characterizes a fundamental aspect of energy dissipation in a flow–obstacle system. The role of the magnetic field is clearly determinant: a non–magnetized flow interacting with a non–magnetized obstacle does not lead to electron acceleration and associated electromagnetic emissions. Thus, even is the SW-magnetosphere interaction, dominated by the incident kinetic flow power, the IMF plays a crucial role for extracting part of the flow power and converting it to energetic particles (e.g. through reconnection). The similar values of ε in equations (5 & 9) and of $(1 + M_{\rm A}^{-2})^{-1/2}$ in equation (8), and the single value – or limited range – of efficiency η in all configuration, express that a similar fraction of the incident Poynting flux can be extracted in all three underlined cases of Table 1 and used for accelerating electrons, even if the details of the extraction process differ: field line draping followed by reconnection in the magnetospheric interaction, reconnection without draping in the dipolar interaction, and Alfvén waves in the unipolar interaction. In any case, we will consider in the following the "generalized Radio–Magnetic Bode's law" defined by equations (9 & 10) as a factual result that we will extrapolate and apply to exoplanets.

When applying equations (9 & 10) to the interaction of the moon Dione with Saturn's magnetic field, we obtain $P_{\rm d} \sim 4 \times 10^8$ W and $P_{\rm Radio} \sim 0.7 - 4 \times 10^6$ W, i.e. <1% of Saturn's auroral kilometric radiation power (see Figure 6). The influence of Dione on Saturn's radio spectrum, suggested by Voyager observations (Kurth et al., 1981; Desch and Kaiser, 1981), seems thus unlikely. If confirmed by the analysis of long-term measurements from Cassini, it would imply an electromagnetic cross section for Dione one order of magnitude larger than the size of its disk, due to an intrinsic magnetic field or more probably to an extended exosphere.

Although Table 2 may suggest that a "UV–Magnetic Bode's law" could also be defined, this proves to be difficult because (*i*) the main auroral ovals at the various planets have different physical origins (SW coupling/reconnection at Earth, corotation breakdown at Jupiter, Kelvin-Helmholtz waves or field-aligned currents at Saturn's magnetopause...), and (*ii*) the radiated UV power depends not only on the nature and energy of precipitated particles, but also on atmospheric composition and radiative transfer. Thus, a correlation valid for various emissions at one single planet (as in Table 2) cannot necessarily be generalized to all auro-

ral UV emissions. By contrast, radio emissions at all planets are directly emitted by precipitated (or mirrored) electrons with energy 1–10 keV, and in Figure 6 each radio component was related – as far as possible – to the corresponding flow–obstacle interaction driving it (e.g. only the hecto–decameter emission independent of Io was used for $P_{\rm Radio}(J)$, etc.). From the point of view of detectability, we have seen in section 1 that the planet–star contrast is much more favourable in radio than in UV.

5. The case for "hot Jupiters"

Out of ∼170 exoplanets known at the time of this writing (within 146 planetary systems – cf. (Schneider, 2006)), 27 (16%) have a semi–major axis ≤0.05 AU (or ∼10 $R_{\rm S}$, with $R_{\rm S}$=7×10^8 m the solar radius and 1 AU = 213.7 $R_{\rm S}$), and 39 (23%) have a semi–major axis ≤0.1 AU. These planets are called "hot Jupiters" due to their strong irradiation. As noted by Zarka et al. (2001a), these planets, when orbiting a solar–type star, receive from the wind of their parent star an energy flux 10^3 to 10^5 times larger than at Jupiter's orbit. Stronger stellar wind would of course lead to still higher power inputs.

By analogy with the solar wind, the stellar wind plasma is expected to carry away frozen–in magnetic field from the star through the circumstellar medium. In the case of the Sun, the large scale dipolar field has a surface intensity about 1 to 1.5 G. Magnetic spots and associated loops may exhibit magnetic field intensities of 10^3 G on a few percent of the solar surface (Priest, 1995). Stellar surface magnetic fields of the order of 10^3 G are not uncommon (so–called magnetic stars) (see e.g. Saar, 1996).

Exoplanets may have a strong (Jovian–like) magnetic field, but they may also be weakly magnetized or unmagnetized due to tidal spin–orbit synchronization. All empirical laws used for estimating planetary magnetic dipole fields generated by the planetary dynamo involve a term $P_{\rm sid}^{\alpha}$ where $P_{\rm sid}$ is the sidereal planetary rotation period and $-1 \leq \alpha \leq -1/2$ (see appendix of Farrell et al., 1999). The predicted planetary field is thus expected to decrease with increasing sidereal rotation period. For hot Jupiters, strong tidal interactions are expected to lead quickly (in 10^{6-7} years) to planetary spin–orbit synchronization, and thus to sideral rotation slowing down (to 3–4 days) and decay of the magnetic moment. A recent study by Sanchez–Lavega (2004) based on internal structure and convection models predicts upper limits of 1.5 to 6 G for the surface field of hot Jupiters (versus 8.5 G for Jupiter's dipole field).

The type of star–planet "plasma" interaction will of course strongly depend on the magnetic field of each of the two bodies involved. We examine below the three cases (underlined in Table 1) potentially leading

to intense CMI radio emission, in the frame given by equations (1, 3, 9 & 10).

5.1 Magnetospheric interaction

If the planet is strongly magnetized (surface field above a few Gauss), then it will have a developed magnetosphere interacting with the stellar wind in a way similar to the Earth's or Jupiter's magnetosphere with the solar wind.

Following Zarka et al. (2001a), we can estimate the dissipated powers for exoplanets around a solar–type star (with a solar–type stellar wind) just based on the dependence of SW parameters (N, B, V) with the distance d to the Sun. To a first approximation, beyond a few R_S above the solar surface, V can be considered as constant, the density N and radial field B_r vary in $1/d^2$, and azimuthal field B_φ in $1/d$ (see section 3). For a better description close to the Sun, we have used the following expressions adapted from Hollweg (1999):

$$\begin{array}{ll} B_r(G) & = 1.5/d^2 \times (1 + (f-1)/d^{1.5}) \\ B_\varphi & = B_r \times \Omega d/V \\ B_{\rm tot} & = (B_r^2 + B_\varphi^2)^{1/2} \end{array} \qquad (11)$$

with $4 \leq f \leq 9$ the non–d^2 expansion factor (we use f=6.5), and d expressed in units of solar radii, and

$$N_{\rm e}({\rm cm}^{-3}) = 3 \times 10^8 d^{-15} + 4 \times 10^6 d^{-4.5} + 2.3 \times 10^5 d^{-2} \qquad (12)$$

providing $N_{\rm e} = 5$ cm^{-3} at the Earth orbit ($d = 1$ UA $= 214\ R_S$). Figure 7 shows the corresponding profiles for $B_{\rm tot}(d)$ and $N_{\rm e}(d)$. The profile $V(d)$, plotted on Figure 8, has been deduced from energy density plots by Shatten (1972). Other descriptions of B, N and V can be found in the literature but our results below are little dependent on the detailed formulas used.

The term $B_\perp$ entering equation 9 is the SW magnetic field perpendicular to the flow in the planet's frame. Similarly, V represents the SW flow velocity in the planet's frame. For orbital distances of 1 to several AU, the flow direction can be taken along the Sun–planet line and the planetary orbital speed can be neglected relative to the flow speed ($V_{\rm SW}$ in the Sun's frame). This is no more true for hot Jupiters at 0.05–0.1 AU orbital distance. Figure 8 displays the orbital velocity $V_{\rm orb} = (G{\rm M_S}/d)^{1/2}$ versus the distance to the Sun, the flow speed $V_{\rm SW}$, and the "effective" flow velocity in the planet's frame $V = V_{\rm SW} - V_{\rm orb}$). Due to the large orbital velocities close to the Sun, V remains everywhere above $\sim$ 300

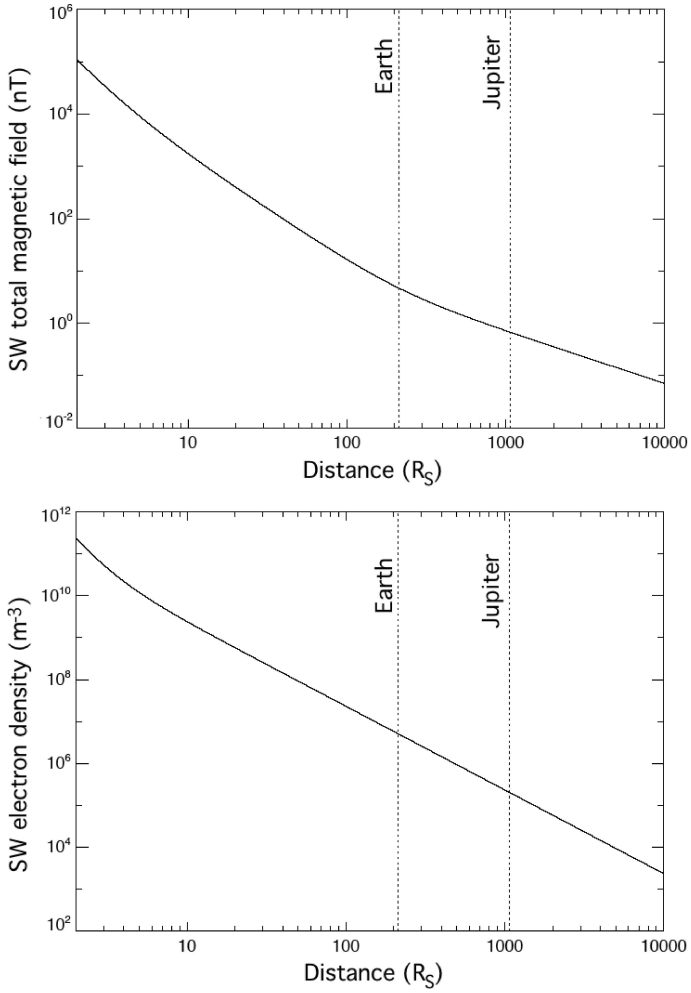

Figure 7.: *Typical profiles of the total SW magnetic field ($B_{\rm tot}$, top) and electron density ($N_{\rm e}$, bottom) versus distance to the Sun (see text). $R_{\rm S}$ is the solar radius (1 $R_{\rm S} = 7 \times 10^8$ m). Orbits of the Earth (1 AU = 213.7 $R_{\rm S}$) and Jupiter (5.2 AU = 1111 $R_{\rm S}$) are indicated.*

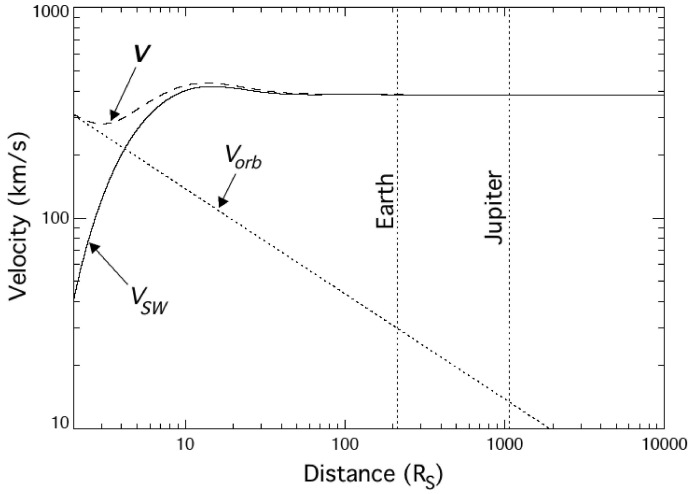

Figure 8.: *Typical SW velocity profile (see text).* $V_{\rm SW}$ *is the flow speed in the Sun's frame,* $V_{\rm orb}$ *the Keplerian orbital velocity versus distance, and* V *the resulting SW flow velocity in the planet's frame. Note that the latter remains high even close to the Sun.*

km/s instead of steeply decreasing below $\sim 10{\rm R_S}$. $B_\perp$ is then calculated as:

$$B_\perp = B \times |\sin(\alpha - \beta)| \tag{13}$$

with $\alpha = {\rm arctg}(B_\varphi/B_r)$ and $\beta = {\rm arctg}(V_{\rm orb}/V_{\rm SW})$

Figure 9a displays a sketch of the corresponding geometry, and Figure 9b shows plots of $\alpha(d)$ and $\beta(d)$. Figure 10 displays variations of $|\mathbf{B}|$, B_φ, B_r, and $B_\perp$ versus the distance. Far from the Sun $B_\perp$ varies as B_φ (i.e. in $1/d$) while close to the Sun, $B_\perp$ varies as B_r (i.e. in $1/d^2$). In between, at $d \sim 37{\rm R_S}$, $B_\perp$ goes through a deep minimum where the effective flow velocity is along the Parker spiral.

It is then easy to compute the dissipated magnetic power per unit area ($VB_\perp^2/\mu_0$), plotted versus distance on Figure 11. On the same figure the dissipated kinetic (flow) power per unit area (NmV^3) is superimposed. We note that the magnetic power becomes comparable to the kinetic one at about 10 $\rm R_S$ distance, while their ratio is constant and ~ 170 beyond about 100 $R_{\rm S}$ (~ 0.5 AU). The kinetic power at the orbit of a hot Jupiter (0.05 AU) is found 2×10^4 times larger than at Jupiter's orbit (at 5.2 AU), and this ratio is 6×10^5 for the magnetic power.

A magnetized hot Jupiter will thus experience a much stronger magnetospheric interaction than Jupiter's one. But magnetospheric compres-

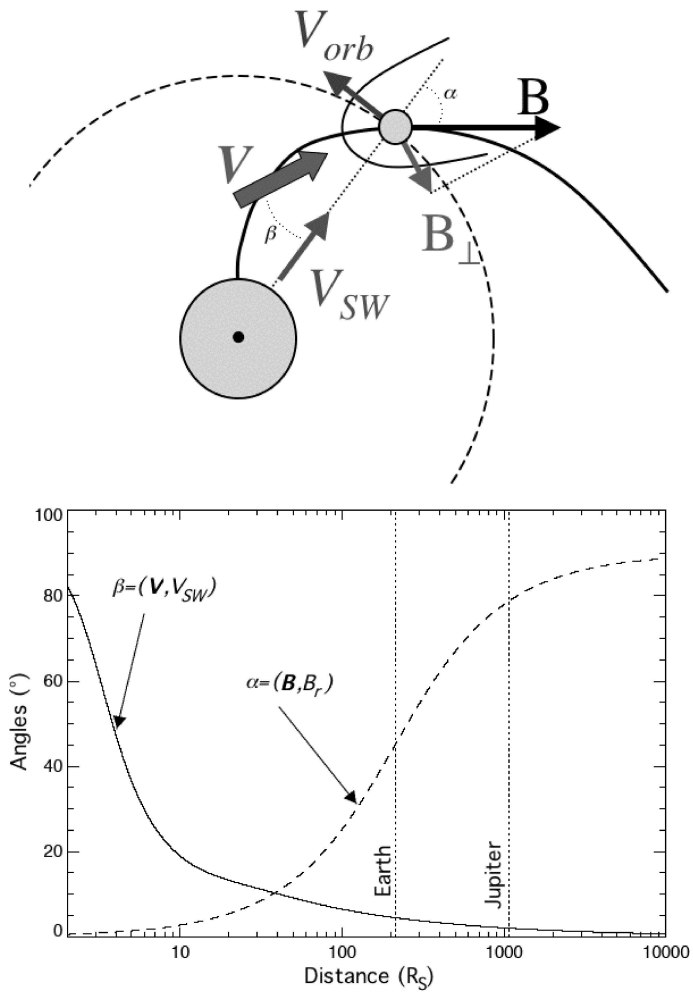

Figure 9.: *(a) Sketch of the geometry of the SW flow and magnetic field at a planetary orbit. The IMF (**B**) is tangent to the Parker spiral. $B_\perp$ is the SW field perpendicular to the flow in the planet's frame, which enters in the IMF Poynting flux onto the magnetospheric cross–section. (b) Variation of the angles defined in the figure (and in section 4 .1) versus distance to the Sun.* ***V*** *and* ***B*** *are aligned at* $d \sim 37\ R_S$.

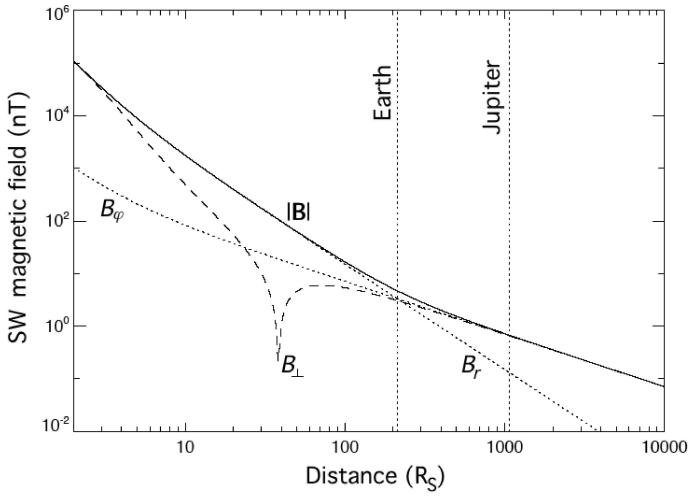

Figure 10.: *Variations with distance of total IMF magnitude* $|\boldsymbol{B}|$*, azimuthal and radial components* B_φ*,* B_r*, and perpendicular component* $B_\perp$*.*

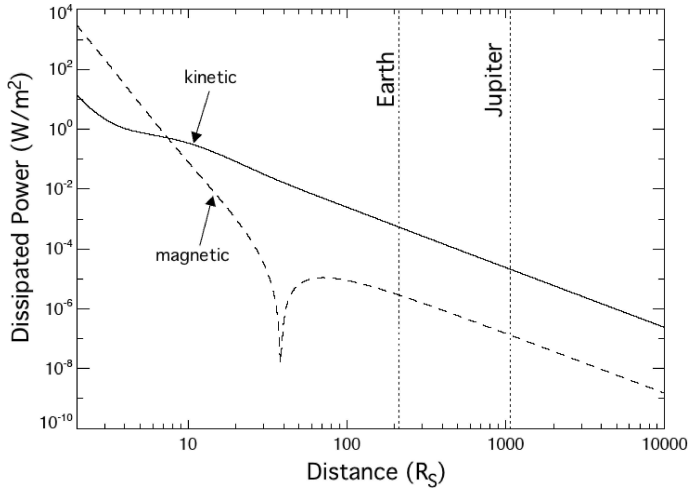

Figure 11.: *Dissipated SW magnetic power* $(VB_\perp^2/\mu_o)$ *and kinetic power* (NmV^3) *per unit area. Both become comparable at a distance about 10* $R_{\rm S}$*.*

sion must also be taken into account (equation 4). The much higher pressure at 0.05 AU results in a highly compressed magnetosphere (by a factor ~ 5), as illustrated on Figure 12 for a planetary magnetic field equal to Jupiter's. Finally, the dissipated (magnetic) power as defined by equation (9) is $6 \times 10^5/5^2 = 2.4 \times 10^4$ times larger for a Jovian–like hot Jupiter at 0.05 AU than for Jupiter itself. This factor largely exceeds 10^5 for the closest hot–Jupiters (at 0.02–0.03 AU from their parent star). If kinetic input power to the magnetosphere is considered (equation (3)), the gain is only a factor $\sim 10^3$ relative to Jupiter (Figure 13).

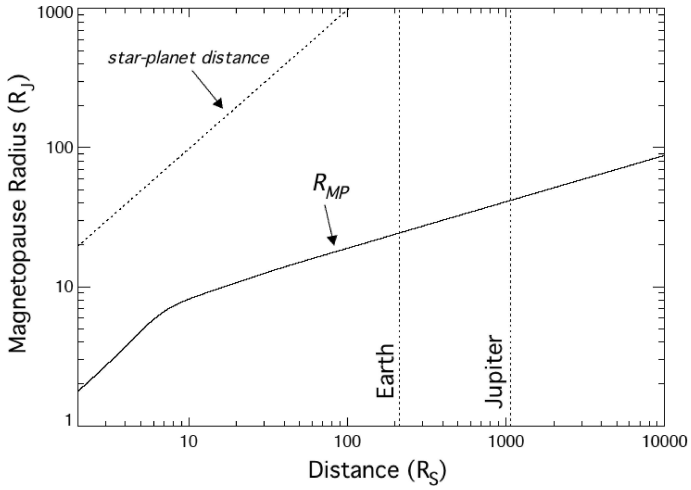

Figure 12.: *Radius of the magnetopause cross–section versus the distance to the Sun for a planet with magnetic dipole equal to Jupiter. At 10 R_S, the magnetosphere is compressed by a factor ∼5 relative to Jupiter's magnetosphere at 5 AU. For a Jovian–like field, the magnetosphere of a hot Jupiter remains much smaller than the star–planet separation at all orbital distances.*

Extrapolation of the generalized Radio–Magnetic Bode's law of Figure 6 using the above dissipated powers imply that hot Jupiters may produce radio emissions 10^3 to 10^5 times more intense than Jupiter, if no unexpected "saturation" mechanism occurs which would prevent to reach such high radio fluxes.

5.2 Dipolar interaction

If in addition the stellar wind is strongly magnetized , the star–planet interaction will be "dipolar" and will involve reconnection at the magnetopause as discussed above in the Ganymede–Jupiter case. Its strength can be evaluated according to equation (9) (with $\varepsilon = 1$), as

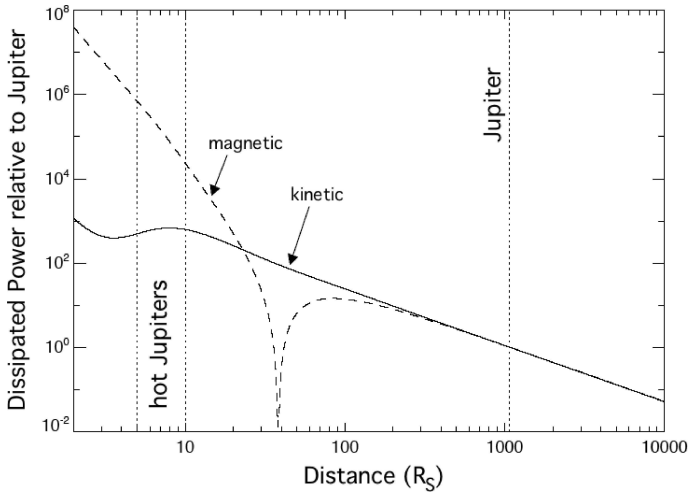

Figure 13.: *Dissipated SW magnetic and kinetic powers for a Jovian–like hot Jupiter, relative to the case of Jupiter itself. For hot Jupiters, the ratio for kinetic powers is* $\sim 10^3$ *while it exceeds* $2{\times}10^4$ *for magnetic powers (up to several times* 10^5*).*

already suggested by Zarka et al. (2001a). Making an analogy with RS CVn magnetic binary stars, Cuntz et al. (2000) and Saar et al. (2004) evaluated the reconnected power in a slightly different manner, also proportional to the magnetic energy density (thus to B^2) at the interaction point, and to the relative velocity between the interacting magnetic field lines.

The dissipated power can be estimated as above via equation (9): it is that of the magnetospheric interaction multiplied by a factor $\sim (B_{\rm star}/B_{\rm Sun})^2$, thus possibly largely exceeding a factor 10^6 relative to Jupiter. In the above two cases, electrons accelerated through the SW–planet interaction can precipitate along the planet's magnetic field lines towards its auroral regions and produce there intense radio emissions at decameter wavelengths.

5.3 Unipolar interaction

If the planet is weakly magnetized or unmagnetized, it will still drive an electrodynamic interaction with the star's magnetic field, similar to the Io–Jupiter interaction, with the star playing the role of Jupiter and the exoplanet that of Io. The similarity is further supported by the fact that the solar wind becomes sub–Alfvénic below about 15 $R_{\rm S}$ ($\sim$ 0.07 AU) from the Sun, according to equations (11–12). Figure 14 displays

the Alfvén Mach number $M_{\rm A} = V/V_{\rm A} \approx V \times (1.1 \times \mu_0 N m_{\rm p})^{1/2}/B_{\rm tot}$ as a function of the distance to the Sun. In the case of a magnetic star, the sub–Alfvénic zone extends farther than in the solar case ($\propto B_{\rm star}/B_{\rm Sun}$). The system formed by a weakly magnetized hot Jupiter and its magnetized parent star is thus a giant analogous to the Io–Jupiter system. Through its induced magnetic field or UV–induced ionosphere, the planet will interact with the star's magnetic field by generating waves (Alfvén, slow mode...), in turn accelerating electrons along field lines towards the star's surface. The dissipated power through this "unipolar" interaction can be again estimated according to equation (9) with $\varepsilon = 1$, and the cyclotron radio power emitted by accelerated electrons along the star's magnetic field lines via equation (10).

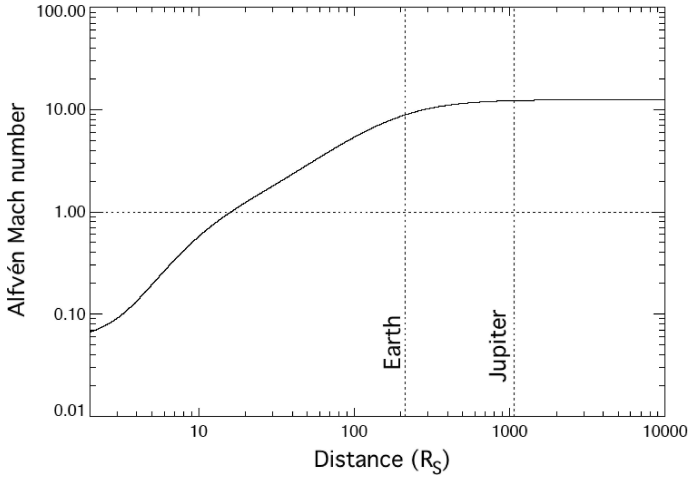

Figure 14.: *Alfvén Mach number function of the distance to the Sun. The SW becomes sub–Alfvénic within about 15 $R_{\rm S}$. In the case of a magnetic star, the sub–Alfvénic zone extends farther than in the solar case ($\propto B_{\rm star}/B_{\rm Sun}$).*

However, an important difference exists with respect to Jupiter. At Jupiter, the ionospheric plasma density decreases exponentially above a peak at $N_{\rm e} \sim 3.5{\times}10^5$ cm^{-3} with a topside scale height of $\sim$1000 km (Hinson et al., 1998), while the dipolar magnetic field decreases in $1/R^3$ from a surface value of 4 to 14 G. Thus the ratio $f_{\rm pe}/f_{\rm ce}$ is everywhere $\leq$0.1, the critical threshold value below which efficient wave amplification by the cyclotron–Maser instability is possible (Le Quéau et al., 1985; Zarka, 1998; Zarka et al., 2001b). By contrast, the solar corona has on the average $f_{\rm pe}/f_{\rm ce} \geq 1$, (Figure 15) forbidding thus cyclotron–Maser emission at the fundamental of the X mode, by far the most efficient

process of radio emission generation. Fundamental O mode or second harmonic O and X mode emissions remain possible, but with an efficiency at least 20 to 30 dB lower than fundamental X mode (Ashwanden and Benz, 1988; Treumann, 2000).

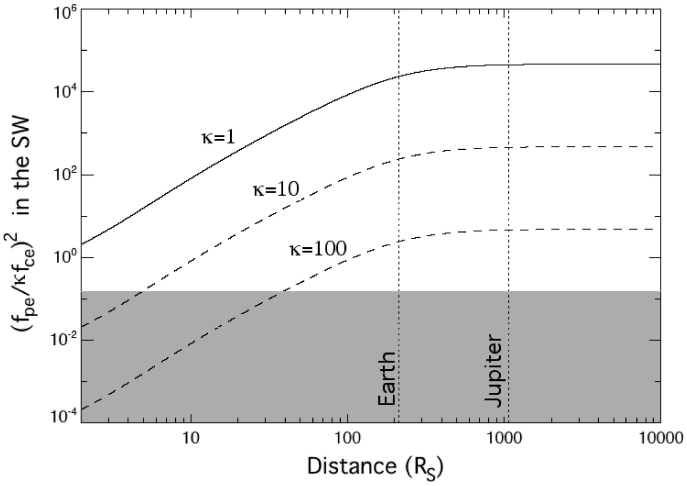

Figure 15.: *Ratio* $(f_{\rm pe}/(\kappa f_{\rm ce}))^2$ *versus distance.* $\kappa = 1$ *for the Sun. Radio wave generation/amplification via the cyclotron–maser mechanism is possible only in the shaded region. Cyclotron–Maser operation at the orbit of hot Jupiters is possible only for stars much more strongly magnetized than the Sun* ($\kappa \sim 100$)*.*

Fundamental X mode emission becomes possible for $f_{\rm ce}$ about 10 to 100 times higher than in the solar case (Figure 15), i.e. restricted to strongly magnetized localized regions of the solar or stellar surface, or in the case of a strongly magnetized star. The two consequences are:
(i) Radio emission will be produced at higher frequency than in the case of magnetospheric interaction, where the expected cyclotron frequencies are or the order of that of Jupiter, i.e. tens of MHz; the cyclotron frequencies derived from equation (11) are between 30 MHz near the solar surface (out of magnetic spots) and ∼3 MHz 1 R_S above it ; in the case of unipolar (or dipolar) interaction with a stellar magnetic field at least 10 times stronger than the Sun's, the radio frequencies emitted by precipitating electrons in the same altitude range above the stellar surface would be $\geq 30 - 300$ MHz.
(ii) The dissipated power can again be estimated via equation (9) and is thus that of the magnetospheric interaction multiplied by a factor $(R_{\rm exo-ionosphere}/R_{\rm magnetosphere})^2 \times (B_{\rm star}/B_{\rm Sun})^2$; the typical radius of the exo–ionosphere of a hot Jupiter is $\sim 2R_{\rm J}$ (see e.g. Vidal–Madjar et

al., 2003) versus $\sim 8R_{\rm J}$ for the magnetosphere of a Jupiter at 0.05 AU (Figure 12), thus for $B_{\rm star} = 10 \times B_{\rm Sun}$, the above multiplying factor is $(2/8)^2 \times (10)^2 \sim 6$.

Unipolar interaction between a hot Jupiter and a magnetic star (or strongly magnetized regions of the stellar surface) is thus expected to produce radio emission up to 10^6 times that of Jupiter at frequencies of tens to hundreds of MHz, again if no unexpected "saturation" mechanism prevents intense radio emission generation (Figure 6).

5.4 Discussion

Farrell et al. (1999) have applied the initial (kinetic) radiometric Bode's law of (Desch and Kaiser, 1984) and (Zarka, 1992) to hot Jupiters discovered before 1999, including planetary magnetic field estimates and the possible effect of radio scintillations (sporadic maxima may reach 100× the average radio power). They inferred that τ Bootes or ρ CrB might be intense decameter radio sources. Lazio et al. (2004) re–applied the same analysis to a more recent exoplanet census. Several recent papers gave a special attention at estimating the stellar wind strength: some authors discussed the use of the stellar X–ray flux $F_{\rm X}$ as a proxy for the wind strength (with a stellar mass loss proportional to $F_{\rm X}^{1.15}$) (Saar et al., 2004; Stevens, 2005), while others attempted to model stellar wind regimes based on observed stellar parameters (Preusse et al., 2005). The temporal evolution of the stellar wind and of the planetary radius was discussed by Griessmeier et al. (2004, 2005) and Stevens (2005), with the conclusion that young systems may offer conditions more favourable than older ones for radio detection (stronger stellar wind and larger planetary obstacle with a more intense planetary field).

The specific case of a unipolar inductor system including a magnetic white dwarf and a second body that may be another white dwarf (possibly non–magnetic) or a planet has been studied by Willes and Wu (2004, 2005). More generally, radio flares from magnetic stars, especially if they are periodic, could be driven by the presence of a close–in orbiting exoplanet playing the role of a unipolar inductor. This is the reason invoked by Rubenstein and Schaefer (2000) and Schaefer et al. (2000) to explain the "superflares" with power 10^{23} to 10^{28} W that they have discovered originating from nine solar-type stars. The search for periodicities in the radio emission of known flaring stars could allow to test the presence of a planetary companion.

5.5 The case of HD 179949

Shkolnik et al. (2003) have studied the spectrum of several stars, known from radial velocity measurements to possess a hot Jupiter, to search for periodic variation of chromospheric lines at the planetary or-

bital period. They found such variations (at ∼4% level) in the Ca II H and K lines (393.3 and 396.8 nm) of the star HD 179949, with a period consistent with the 3.093 day revolution period of the planet orbiting it at 0.045 AU. The star's rotation period was estimated to be about 6–10 days. They interpreted this periodic variation of the chromospheric activity as driven by magnetic reconnection between the magnetic fields of the two bodies (similar to our above dipolar interaction), leading to charged particles precipitation towards the star's surface and resulting in a chromospheric hot spot (tidal interaction was ruled out because it should lead to 2 maxima per planetary revolution – cf. Cuntz et al. (2000)). The hot spot was tentatively found to lie $\sim 60°$ longitude ahead of the planet's orbital position. As the planet is likely to be tidally spin–orbit synchronized, its magnetic field may be weak, actually resulting in a unipolar inductor–like interaction. We comment here two aspects of HD 179949: the dissipated power and the longitudinal shift of the hot spot.

The maximum dissipated power can be estimated again from equation (9) setting ε=1. From Figure 11, we derive a magnetic power flux ∼0.15 W/m^2, and a kinetic (flow) power flux 3 times as high, at an orbital distance of 0.045 AU or 9 R_S. The maximum dissipated power per Jovian radius of the obstacle is thus $\sim 0.15 \times \pi R_J^2 = 2 \times 10^{15}$ W. How does this number compare to the power radiated by a chromospheric spot increasing the star's brightness by 4% in the Ca II H and/or K lines ? Solar optical brightness is $\sim 10^{13}$ Wm^{-1}m^{-2}sr^{-1}, so that the power P corresponding to 4% of the intensity of a 0.3 Angström–wide line of intensity being ∼1/3 of the stellar continuum (Shkolnik et al., 2003) is:

$$P \sim 10^{13} \times 0.3 \times 10^{-10} \times 2\pi^2 R_S^2 \times 0.04/3 \sim 4 \times 10^{19} \mathrm{W}$$

The available power appears thus several thousand times lower than the radiated one. The resolution of this problem would require a stellar magnetic field ∼30–100 times more intense than the solar one, or a wind strength much larger than the Sun's, or an obstacle size much larger than πR_J^2 due to a strong intrinsic planetary field or an extended exo–ionosphere, or a combination of several of these factors. Shkolnik et al. (2003) mentioned that, in the case of HD 179949, F_X is likely to be 10 times that of the Sun. As discussed in the previous section, existence of a radio emission associated with this possible magnetic star–planet interaction depends on the existence of a strong planetary or stellar magnetic field.

The same power problem is much more severe for the superflares of Schaefer et al. (2000). The estimated powers of 10^{23} to 10^{28} W would require unreasonably large stellar magnetic fields for the solar type stars

involved, and extremely large planetary obstacles very close to their parent star.

Coming back to HD 179949, the 60° lead angle of the chromospheric hot spot relative to the sub–planet point raises another problem: the lead angle of the Io–induced UV/infrared/Radio emissions relative to Io's instantaneous longitude is most of the time positive because Jupiter'rotation period is shorter than Io's orbital period so that the "downstream" direction in the Io–Jupiter interaction is ahead of Io's relative to its orbital motion. But in the case of HD 179949, the planetary orbital period is much shorter than the estimated stellar rotation. If induced by the planet, the chromospheric hot spot should lag the instantaneous longitude of the planet (in the star's frame). The observed lead angle may be explained by a combination of the following effects:

- the Parker's spiral at 0.045 AU, which implies (with $V \sim 400$ km/s) a longitude shift of $+10°$ between the point of the stellar surface magnetically connected to the planet and the planet itself ;
- a distorted stellar magnetic field geometry (non–meridian field lines) consistent with the fact that HD 179949 is a rapid rotator (6–10 day period);
- a tilt between the star's rotation axis and magnetic dipole axis.

However the latter two effects should lead to alternatively positive and negative longitude shifts, difficult to reconcile (even with a selection effect of the observations) with an apparently stable lead angle of 60°.

Thus, the observations of Shkolnik et al. (2003) raise problems in terms of both the dissipated power and the longitudinal shift of the chromospheric hot spot. We consider thus (in agreement with Saar et al. 2004) that this first detection of a planet–driven chromospheric activity still requires confirmation.

6. Radio observations

6.1 Sensitivity and detectability

As can be seen from Figure 1, the LF sky background is a very bright extended source. Its temperature can be represented by

$$T(K) \sim 1.15 \times 10^8 / f^{2.5}$$

with f in MHz (Van Haarlem et al., 2001). In the range $10 \leq f \leq 100$ MHz, $T \sim 10^{4-6}$ K. The amplitude of spatial variations across the sky is a factor 2 to 3. The detected flux density from an extended source is:

$$S(\mathrm{Wm^{-2}Hz^{-1}}) = B\Omega = 2kT/A_\mathrm{e}$$

with

$$B(\mathrm{Wm^{-2}Hz^{-1}sr^{-1}}) = 2kT/\lambda^2$$

the sky brightness and Ω the radiotelescope main beam ($A_\mathrm{e}\Omega = \lambda^2$) (Kraus, 1986). The RMS amplitude of the sky background noise fluctuations, which will ultimately limit the sensitivity of the observations, is:

$$\sigma = \frac{2kT}{A_\mathrm{e}\sqrt{b\tau}} \tag{14}$$

with A_e the effective area of the radiotelescope, b the bandwidth and τ the integration time of the observations. The signal to noise ratio is thus $N = S/\sigma$, where we can normalize the signal S relative to the maximum flux density of intense Jovian bursts at 1 AU range, $S_\mathrm{J} \sim 10^{-18}$ $\mathrm{Wm^{-2}Hz^{-1}} = 10^8$ Jy: $S = \zeta \times S_\mathrm{J}/d^2$ with d the distance of the target in AU, and ζ the intrinsic signal intensity normalized to Jupiter's. The maximum distance at which a radio emission of flux density $\zeta \times S_\mathrm{J}$ can be detected at the $N\sigma$ level is thus:

$$d_\mathrm{max} = \sqrt{\frac{\zeta S_\mathrm{J} A_\mathrm{e}}{2NkT_\mathrm{s}}}(b\tau)^{1/4}$$

hence with N=3,

$$d_\mathrm{max}(\mathrm{pc}) = 5 \times 10^{-8}(A_\mathrm{e}\zeta)^{1/2} f^{5/4}(b\tau)^{1/4} \tag{15}$$

Using a moderately high "gain factor" $\zeta = 10^5$ (from the scaling laws of section 5), we obtain in Table 3 values of d_max for various realistic observation parameters. The results are one order of magnitude smaller for $\zeta = 10^3$. A large effective area appears to be necessary to overcome the sky background fluctuations, restricting exoplanet radio search to large ground–based radiotelescopes.

In addition to the ultimate sensitivity limit set by σ, other limiting factors are natural and man–made RFI, and ionospheric propagation effects (strong scintillation for frequencies below a few times the Earth's ionospheric cutoff frequency, i.e. typically for $f \leq 30$ MHz). The former are broadband and impulsive (e.g. lightning) or narrowband (artificial transmitters) signals that may peak several tens of dB above the exoplanetary signals searched for. Thus, the relatively broad bandwidth required in Table 3 must be recorded with high–spectral resolution and be followed by powerful (online and/or offline) RFI suppression processing

Table 3.: *Maximum distance of detectability (in pc) as a function of radiotelescope area, observation frequency, bandwidth and integration time, for $\zeta = 10^5$, as deduced from equation (15). Examples of radiotelescopes are given in italics, as well as typical values of b and τ for the corresponding product $b\tau$. The results are one order of magnitude smaller for $\zeta = 10^3$.*

	b $\tau = 10^6$ *(1 MHz, 1 sec)*		b $\tau = 2{\times}10^8$ *(3 MHz, 1 min)*		b $\tau = 4{\times}10^{10}$ *(10 MHz, 1 hour)*	
	f = 10 MHz	f = 100 MHz	f = 10 MHz	f = 100 MHz	f = 10 MHz	f = 100 MHz
$A_e = 10^4$ m^2 *(NDA)*	1	16	3	59	13	220
$A_e = 10^5$ m^2 *(UTR–2)*	3	50	11	190	40	710
$A_e = 10^6$ m^2 *(LOFAR)*	9	160	33	600	130	2200

before numerical spectral integration. Mitigation of ionospheric propagation effects requires an extended and flexible instrument (e.g. with multi–beam capability) and specific calibration/correction algorithms.

6.2 Ongoing searches

Tables 4 and 5 list the main characteristics of a few representative large ground–based LF instruments relevant for exoplanet radio search. All are phased arrays (allowing to derive absolute fluxes) or interferometers. Frequency ranges are covered fully (NDA, UTR–2), in parts (LOFAR), or only as discrete narrow bands (VLA, GMRT). Beam sizes depend on the configuration of the array and sensitivity on integration time and channel bandwidth, so that only typical representative numbers are given. See references for details. By using modern digital receivers and real–time RFI–mitigation techniques, modest–size instruments as the NDA can nevertheless achieve powerful observation capabilities, and even be able to detect exoplanetary signals if emissions $\geq 10^5$ times Jupiter's effectively exist.

As 1 AU at 1 pc corresponds by definition to a separation of 1", source imagery is not adapted to the LF radio range. Ongoing radio searches thus intend to (i) detect a signal, and (ii) distinguish between a stellar or planetary origin for which comparable intensities are expected. Planet identification will rely upon the measurement of circular or el-

Table 4.: *Characteristics of large ground–based instruments used for exoplanet LF radio search : NDA, VLA, GMRT, UTR–2, and LOFAR.*

Instrument Name & Location	NDA (Nançay Decameter Array), France	VLA (Very Large Array), New Mexico, USA	GMRT (Giant Meterwave Radio Telescope), Pune, India
References	*Boischot et al., 1980 ; Lecacheux et al., 2004*	*Kassim et al., 1993 ; Cotton & Condon, 2002*	*Swarup, 1990*
Description	2×72 helix-spiral antennas rectangular arrays	Interferometer: 27 parabolas × 25m ⊘ Y-shape array	30 parabolas × 45m ⊘ core + Y-shape arr.
Frequency range (MHz)	10 – 100	74 (±0.75), 330, ...	(50), 150, 235, ...
Effective area (m^2)	$\sim 2 \times 4000$	~ 13000	~ 30000
Beam	$\sim 6^\circ \times 10^\circ$	≥ 0.4'	0.3'
Polarization	2 circular → 4 Stokes	2 polar.	4 Stokes
Maximum effective sensitivity (Jy)	$\sim 10^2$	10^{-1}– 10^{-2}	10^{-2}– 10^{-3}

Instrument Name & Location	UTR–2 (Ukrainian T–shape Radiotelescope, Mark 2), Kharkov, Ukraine	LOFAR (Low Frequency Array), The Netherlands
References	*Braude et al., 1978 ; Konovalenko, 2000*	*Van Haarlem et al., 2001 ; Kassim et al., 2004*
Description	2040 dipoles (T–shape array)	Interferometer / Phased arrays of dipoles (core + stations up to ≥200 km)
Frequency range (MHz)	7 – 35	(10) 30 – 240 in eight 4 MHz bands
Effective area (m^2)	~ 140000 (NS: 1800×60, EW: 900×60)	$\sim 10^6 \times (15/\nu)^2$
Beam	$\sim 30' \times 10^\circ$	$1.5'' \times (100/\nu)$ [ν in MHz]
Polarization	1 linear polar. (EW)	4 Stokes
Maximum effective sensitivity (Jy)	10^0– 10^1	$\leq 10^{-3}$

liptical polarization in the incident radiation (solar bursts are generally unpolarized), or upon an observed periodicity of the emission at a period either of a few hours (Jupiter–like) or equal to the orbital period of the planet.

Observations of hot Jupiter targets started in 1996–97 at UTR–2 using a acousto–optical spectrograph (AOS (Raterron, 1985)). Observation band was 10 MHz around a center frequency about 25 MHz, with 30 kHz resolution (333 channels, sampled simultaneously). UTR–2 permits to measure only one linear (EW) polarization, but also to have two or more beams simultaneously in the sky, and thus to perform simultaneous On/Off observations. Jupiter–like bursts were specifically looked for, using an integration time $\tau = 20 - 300$ msec per spectrum, much shorter than the characteristic times of ionospheric fluctuations (10–20 sec) and of AOS gain fluctuations ($\sim$ 1 min), allowing thus to deconvolve the latter during the post–processing of the recorded dynamic spectra. The RFI mitigation processing is described in Zarka et al. (1997). One major limitations of the achieved sensitivity was related to the limited dynamic range of the AOS ($\sim$ 25 dB), coupled to the telescope large beam size (see Table 4) which increases vulnerability to RFI (and confusion with background sources). Extensive analysis of the observations performed in "quiet" conditions (winter nights) between 1999 and 2002 showed that RFI could be efficiently reduced/suppressed by post–processing (Zarka et al., 1997, 2002; Ryabov et al., 2004a,b), but that the ionospheric scintillations near solar maximum activity are another major perturbation, generating ghost emissions by scintillation of remote radio sources through the ionosphere.

Time dispersion of broadband bursts due to chromatic group velocity must be taken into account for LF radio exoplanet search:

$$\delta t(f) = t_{\rm arrival}(f) - t_{\rm arrival}(f \to \infty) = 4.15 \times 10^3 (DM)/f^2 \qquad (16)$$

with δt in seconds, f in MHz, and $(DM) = \int N_{\rm e}.dL$ the dispersion measure along the wave path in pc.cm^{-3}. Typical distances of known exoplanets are in the range 5–100 pc, and the average electron density in the local interstellar medium is $< N_{\rm e} >= 0.03 - 0.08$ cm^{-3}, thus $(DM) = 0.15 - 8$. The differential delay between $f = 20$ MHz and $f = 30$ MHz is thus 1 to 45 sec and must be corrected after RFI suppression and before spectral integration (see Table 2 of Zarka et al. 1997, which also shows that temporal broadening of bursty signal should always be ≤ 100 msec and can thus be neglected). This correction was applied with (DM) as a free parameter, and actually used as a confirmation test in case of detection of a burst in the "On" channel: a real signal is expected to provide a maximum detection only for a restricted range of (DM) consistent with

the target distance. This technique was associated to data accumulation (Ryabov et al., 2004a) and synchronous detection algorithms (see Saar and Cuntz, 2001) searching for weak periodic signals (e.g. at the planetary orbital period). A sensitivity of ~ 1 Jy was reached for observations in "quiet" conditions at UTR–2, and tested through the successful detection of single pulses of weak pulsars. No positive unambiguous detection of an exoplanetary signal was obtained at UTR–2 (Ryabov et al., 2004b).

Other searches have been conducted with the VLA at 74 and 330 MHz. The best candidate of the Farrell et al. (1999) paper, τ Bootes, was observed in 1999 and 2002 (Farrell et al., 2003, 2004b; Lazio et al., 2004). Spatial maps were obtained, with a sensitivity of 0.3 Jy at 73 MHz in 1999, and 0.12 Jy at 74 MHz in 2002 (with 15 min integration). Again, no detection was obtained. Other candidates were unsuccessfully observed at higher frequencies by Bastian et al. (2000). An exoplanet search campaign is also in progress at the GMRT at 150 MHz (Winterhalter et al., 2005).

Although results of observational searches are still negative (Zarka et al., 1997, 2002 ; Ryabov et al., 2004a,b; Farrell et al., 2003, 2004b; Lazio et al., 2004; Bastian et al., 2000; Winterhalter et al., 2005), upper limits of undetected emissions are steadily getting down (cf. Tables 4), closer to predicted fluxes. The sensitivity limits for UTR–2, VLA and GMRT observations are plotted on Figure 1, illustrating the detection capability of these instruments compared to our predictions. Positive results crucially depend on the existence of exoplanetary radio emissions significantly more intense than Jupiter's ($\zeta > 10^3$) at frequencies above the Earth's ionospheric cutoff (implying a magnetic field > 4 G in the source).

The absence of detection until now may be attributed to various causes:

- emission is produced in frequency bands different from those observed: the stellar and planetary fields in the observed systems are either below a few Gauss, or $\gg$50 G;
- the signal is intrinsically weaker than predicted by the above scaling laws, below the effective sensitivity of the instruments used (due to instrument size, receiver stability, confusion...);
- signals are intrinsically intermittent (as Jovian decameter emissions – cf. Figure 2) and were "missed" due to insufficient time coverage of $P_{orbital}$ during observational campaigns.

And more specifically at UTR–2 :

– RFI were not completely suppressed by post–processing, or conversely exoplanetary signals were identified and removed as interference;

– the high level of ionospheric perturbations near solar maximum created spurious "ghost" signals and prevented optimal RFI suppression and weak signal detection;

– the signal detection algorithms (synchronous detection of broadband bursts after dedispersion) does not match the (unknown) characteristics of the exoplanetary signal (e.g. intrinsic bursts drift in addition to interstellar dispersion...).

6.3 Future observations

Increasing computing power allows a better RFI mitigation processing of GMRT and UTR–2 spectral observations. The basic underlying idea of our present method of exoplanet radio search is to choose observation parameters b_0 and τ_0 small enough for ensuring that the maximum expected signal intensity is smaller than sky background fluctuations ($S \ll \sigma_0$). RFI suppression then consists in recognizing in the dynamic spectra recorded with high resolution all pixels higher (e.g. at 3σ level) than the local average (taking into account the instrument response and ionospheric scintillations – τ_0 must be much shorter than the typical timescale of these fluctuations). These pixels recognized as spurious are then masked out before spectral and temporal integration to final bandwidth $b \gg b_0$ and integration time $\tau \gg \tau_0$, which reduces background fluctuations $\sigma = \sigma_0 \times (b/b_0)^{1/2} \times (\tau/\tau_0)^{1/2}$, so that $S \gg \sigma$. Figure 16 illustrates the performances of present algorithms.

Future observations are UTR–2 will be carried out with a digital spectrograph allowing for better stability and dynamic range and thus making longer time integrations possible. Observations in pencil–beam mode (correlation of the two branches of the array) reduce confusion and vulnerability to RFI. Ionospheric scintillations should also be reduced during the solar activity minimum of 2006–2007. Finally, the number of hot Jupiter candidates is rapidly increasing (Schneider, 2006) and observation scheduling may be adapted to maximizing the significance of a detection at the orbital period of the target (see Figure 1 of Saar and Cuntz 2001).

Future LF arrays with total effective area $\geq 10^6$ m^2 will improve our capability for radio detection of exoplanets. The most advanced project is LOFAR (the LOw Frequency ARray – see Table 4, and Farrell et al. 2004a), which will include built–in RFI mitigation capabilities and

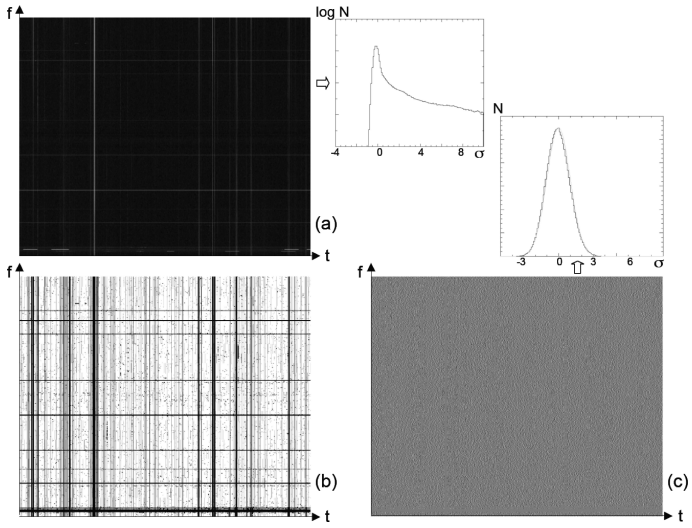

Figure 16.: *RFI mitigation post–processing of digital receiver data from NDA. Dynamic spectrum (a) of the galactic background covers a time interval of 100 sec (5000 spectra × 20 msec/spectrum) and the frequency band 14–28 MHz (2000 frequency channels × 7 kHz). The normalized distribution of intensities* $(I–<I>)/\sigma_I$ *plotted on the right has a high–intensity tail corresponding to RFI. (b) is the map resulting from an automated offline recognition of spurious pixels (in black). (c) = (a) × (b) is the original dynamic spectrum with spurious pixels masked out. Statistical background fluctuations are clearly visible due to the stretched dynamic range of the image. The corresponding distribution of intensities is plotted above it, and is nearly perfectly Gaussian, indicating that all RFI have been effectively suppressed down to the* $\sim 3\sigma$ *level.*

correction for ionospheric propagation effects. Its polarization capabilities will allow to check the planetary origin of the radiation. However, LOFAR will become fully operational not earlier than 2008, i.e. during increasing solar activity (the next maximum will be around 2011).

At higher frequencies, planet–driven radio emissions (through unipolar or dipolar interaction) in the magnetic field of strongly magnetized stars will be searched using SKA and ALMA, as discussed by Willes and Wu (2005) for the case of hot Earths around white dwarf stars.

7. Conclusions

Based on the observed correlation in our solar system between the output planetary radio power and the incident SW power on the magnetopause, and on the energetics of the interaction between Jovian moons and Jupiter's magnetic field, we have derived a "generalized Radio–Magnetic Bode's law" relating the output radio power of a magnetized flow–obstacle system to the Poynting flux (or magnetic energy flux) convected on the obstacle (as defined by equations (9–10)). This flux appears to be the primary engine of such flow–obstacle systems.

Extrapolation of this scaling law to the case of hot Jupiters suggests that these planets may produce very intense cyclotron radio emissions due to either magnetospheric interaction with a strong stellar wind, or to dipolar or unipolar interaction between the planet and a magnetic star (or strongly magnetized regions of the stellar surface). In the former two cases, similar to the magnetosphere–SW interactions in our solar system or to the Ganymede–Jupiter interaction, hecto–decameter cyclotron emission produced in the vicinity of the planet could reach an intensity 10^3 to 10^5 larger than that of Jupiter's LF radio emissions. In the latter case, which is a giant analogous of the Io–Jupiter system, emission in the decameter–to–meter wavelength range near the footprints of the star's magnetic field lines interacting with the planet may reach 10^6 times that of Jupiter (unless some "saturation" mechanism occurs).

The system of HD 179949 might be a good candidate for detection in the radio range, if the planet or the star is strongly magnetized. Discussion of the chromospheric hot spot observed by Shkolnik et al. (2003) in the frame of equation (9) nevertheless raise problems in terms of both the dissipated power and the longitude of the chromospheric hot spot, requiring confirmation of the detection.

The expected favourable planet–star contrast in the LF radio range motivates the actual search of such radio emissions, but the bright galactic background requires the existence of exoplanetary radio emissions significantly more intense than Jupiter's ($\zeta > 10^3$), and the Earth's ionospheric cutoff requires that a substantial part of these emissions is pro-

duced at frequencies $> 10-20$ MHz. As discussed above, a radio emission $> 10^3$ to 10^5 times as intense as Jupiter's decameter emission should be detectable at several tens of parsecs range with present (VLA, UTR–2, GMRT) or future (LOFAR) large ground–based instruments. Beyond LOFAR, a future Moon–based LOFAR–like instrument would give access to radio emissions in the hectometer range (a few MHz) and thus to planets with a weaker magnetic field than Jupiter's (Zarka, 2005).

Finally, there are several interests for the direct radio detection of exoplanets: beyond the mere detection of exoplanetary radio photons, LF radio observations are expected to provide estimates of the planetary magnetic field (putting strong constraints on scaling laws and internal structure models), possibly of the planetary rotation period (confirming or not the spin–orbit locking). They would also provide valuable inputs for extending comparative magnetospheric physics, starting with the validation of the scaling laws such as equation (10).

Acknowledgments. I thank the numerous colleagues with whom I shared work and interest for this topic in the past few years, and especially Tim Bastian, Laurent Denis, Mike Desch, Bill Farrell, Joseph Lazio, Helmut Rucker, Boris Ryabov, Vladimir Ryabov, Rudolf Treumann, and Daniel Winterhalter.

References

[1] Akasofu, S.-I., Energy coupling between the solar wind and the magnetosphere, Space Sci. Rev., 28, 121-190, 1981.

[2] Akasofu, S.-I., Interaction between a magnetized plasma flow and a strongly magnetized celestial body with an ionized atmosphere, Ann. Rev. Astron. Astrophys., 20, 117-138, 1982.

[3] Aschwanden, M. J., and A. O. Benz, On the electron cyclotron Maser instability, II, Pulsations in the quasi-stationary state, Astrophys. J., 332, 446-475, 1988.

[4] Bastian, T. S., G. A., Dulk, and Y. Leblanc, A Search for Radio Emission from Extrasolar Planets, Astrophys. J., 545, 1058-1063, 2000.

[5] Behannon, K. W., Heliocentric distance dependence of the IMF, Reviews of Geophysics and Space Physics, 16, 1978.

[6] Belenkaya, E. S., S. Y.Bobrovnilov, I. I. Alexeev, V. V. Kalegaev, and S. W. H. Cowley, A model of Jupiter's magnetospheric magnetic field with variable magnetopause flaring, Planet. Space Sci., 53, 863-872, 2005.

[7] Boischot, A., C. Rosolen, M. G. Aubier, G. Daigne, F. Genova, Y. Leblanc, A. Lecacheux, J. de la Noë, and B. M. Pedersen, A new high-gain, broadband, steerable array to study Jovian decametric emissions, Icarus, 43, 399-407, 1980.

[8] Braude, S. Ya., A. V. Megn, B. P. Ryabov, N. K. Sharykin, and I. N. Zhouck, Decametric survey of discrete sources in the northern sky: I. the UTR-2 radiotelescope. Experimental techniques and data processing, Astrophys. Space Sci., 54(1), 3-36, 1978.

[9] Cairns, I. H., Solar, interplanetary, planetary, and related extra-solar system science for LOFAR, Planet. Space Sci., 52, 1423–1434, 2004.

[10] Clarke, J. T., J. Ajello, G. Ballester, L. B. Jaffel, J. Connerney, J.-C. Gérard, G. R. Gladstone, D. Grodent, W. Pryor, J. Trauger, and J. H. Waite, Ultraviolet auroral emissions from the magnetic footprints of Io, Ganymede, and Europa on Jupiter, Nature, 415, 997–1000, 2002.

[11] Clarke, J. T., D. Grodent, S. Cowley, E. Bunce, P. Zarka, J. E. P. Connerney, and T. Satoh, Jupiter's Aurora, in Jupiter: The Planet, Satellites, and Magnetosphere, edited by F. Bagenal, W. McKinnon, and T. Dowling., Cambridge University Press, Chapter 26, 639-670, 2004.

[12] Connerney, J. E. P., Doing more with Jupiter's magnetic field, in Planetary Radio Emissions III, edited by H. O. Rucker, S. J. Bauer, and M. L. Kaiser, Austrian Acad. Sci. press, Vienna, pp. 13-33, 1992.

[13] Connerney, J. E. P., M. H. Acuña, N. F. Ness, and T. Satoh, New models of Jupiter's magnetic field constrained by the Io flux tube footprint, J. Geophys. Res., 103, 11929-11939, 1998.

[14] Connerney, J. E. P., R. Baron, T. Satoh, and T. Owen, Images of excited H_3^+ at the foot of the Io flux tube in Jupiter's atmosphere, Science, 262, 1035-1038, 1993.

[15] Cotton, W. D., and J. J. Condon, Calibration and imaging of 74MHz data from the very large array, Proceedings of the URSI General Assembly, 2002.

[16] Cowley, S. H., and E. J. Bunce, Origin of the main auroral oval in Jupiter's coupled magnetosphere-ionosphere system, Planet. Space Sci., 49, 1067-1088, 2001.

[17] Cowley, S. H., E. J. Bunce, and R. Prangé, Saturn's polar ionospheric flows and their relation to the main auroral oval, Ann. Geophys., 22, 1379-1394, 2004.

[18] Cuntz, M., S. H. Saar, and Z. E. Muzeliak, On stellar activity enhancement due to interactions with extrasolar giant planets, Astrophys. J., 533, L151-L154, 2000.

[19] Desch, M. D., Evidence for solar wind control of Saturn radio emission, J. Geophys. Res., 87, 4549-4554, 1982.

[20] Desch, M.D. and M. L. Kaiser, Saturn's kilometric radiation – Satellite modulation, Nature, 292, 739–741, 1981.

[21] Desch, M. D., and M. L. Kaiser, Predictions for Uranus from a radiometric Bode's law, Nature, 310, 755-757, 1984.

[22] Dulk, G. A., Type III solar radio bursts at long wavelengths, in Radio Astronomy at Long Wavelengths, edited by R. G. Stone, K. W. Weiler, M. L. Goldstein, and J.-L. Bougeret, Geophysical Monograph 119. AGU, Washington, DC, pp. 115-122, 2000.

[23] Dungey, J. W., Interplanetary Magnetic Field and the Auroral Zones, Phys. Rev. Lett., 6, 47-48, 1961.

[24] Encrenaz, T.,J. -P. Bibring, M. Blanc, A. Barucci, F. Roques, and P. Zarka, The Solar System (3rd edition), A&A Library, Springer, Germany, 2004.

[25] Erkaev, N.V., Shaidurov, V.A., Semenov, V.S., and Biernat, H.K., Effects of MHD slow shocks propagating along magnetic flux tubes in a dipole magnetic field, Nonlinear Processes in Geophysics 9, 163-172, 2002.

[26] Farrell, W. M., M. D. Desch, and P. Zarka, On the possibility of coherent cyclotron emission from extrasolar planets, J. Geophys. Res., 104, 14025-14032, 1999.

[27] Farrell, W. M., T. J. Lazio, M. D. Desch, T. Bastian, and P. Zarka, Limits on the Magnetosphere/Stellar Wind Interactions for the Extrasolar Planet about Tau Bootes, ASP Conf. Ser., 294: Scientific Frontiers in Research on Extrasolar Planets, 151–156, 2003.

[28] Farrell, W. M., T. J. Lazio, P. Zarka, T. Bastian, M. D. Desch, and B. P. Ryabov, The Radio Search for Extrasolar Planets with LOFAR, Planet. Space Sci., 52, 1469-1478, 2004a.

[29] Farrell, W. M., T. J. W. Lazio, M. D. Desch, T. S. Bastian, and P. Zarka, Radio Emission from Extrasolar Planets, Bioastronomy 2002: Life Among the Stars, Proceedings of IAU Symposium #213, edited by R. Norris and F. Stootman, Astronomical Society of the Pacific, San Francisco, p. 73, 2004b.

[30] Gallagher, D. L., and N. D'Angelo, Correlations between solar wind parameters and auroral kilometric radiation, Geophys. Res. Lett., 8, 1087-1090, 1981.

[31] Galopeau, P., P. Zarka, and D. Le Quéau, Source location of SKR : the Kelvin-Helmholtz instability hypothesis, J. Geophys. Res. -Planets, 100, 26397-26410, 1995.

[32] Genova, F., P. Zarka, and C. H. Barrow, Voyager and Nancay observations of the jovian radio emission at different frequencies : solar wind effect and source extent, Astron. Astrophys., 182, 159-162, 1987.

[33] Goldreich, P., and D. Lynden-Bell, Io: A Jovian unipolar inductor, Astrophys. J., 156, 59-78, 1969.

[34] Griessmeier, J.-M., A. Stadelmann, T. Penz, H. Lammer, F. Selsis, I. Ribas, E. F. Guinan, U. Motschmann, H. K. Biernat, and W. W. Weiss, The effect of tidal locking on the magnetospheric and atmospheric evolution of "hot Jupiters", Astron. Astrophys., 425, 753-762, 2004.

[35] Griessmeier, J.-M., U. Motschmann, G. Mann, and H. O. Rucker, The influence of stellar wind conditions on the detectability of planetary radio emissions, Astron. Astrophys., 437, 717-726, 2005.

[36] Güdel, M., Stellar Radio Astronomy: Probing Stellar Atmospheres from Protostars to Giants, Annu. Rev. Astron. Astrophys, 40, 217–261, 2002.

[37] Gurnett, D. A., W. S. Kurth, A. Roux, S. J. Bolton, and C. F. Kennel, Evidence for a magnetosphere at Ganymede from plasma wave observations by the Galileo spacecraft, Nature, 384, 535-537, 1996.

[38] Gurnett, D. A., A. M. Persoon, W. S. Kurth, A. Roux, S. J Bolton, and C. F. Kennel, Plasma densities in the vicinity of Callisto from Galileo plasma wave observations, Geophys. Res. Lett., 27, 1867-1870, 2000.

[39] Hinson, D. P., J. D. Twicken, and E. T. Karayel, Jupiter's ionosphere: new results from Voyager 2 radio occultation measurements, J. Geophys. Res., 103, 9505-9520, 1998.

[40] Hollweg, J. V., Potential wells, the cyclotron resonance, and ion heating in coronal holes, J. Geophys. Res., 104, 505-520, 1999.

[41] Hospodarsky, G. B., I. W. Christopher, J. D. Menietti, W. S. Kurth, D. A. Gurnett, T. F. Averkamp, J. B. Groene, and P. Zarka, Control of Jovian radio emissions by the galilean moons as observed by Cassini and Galileo, in Planetary Radio Emissions V, edited by H. O. Rucker, M. L. Kaiser and Y. Leblanc, Austrian Acad. Sci. Press, Vienna, pp. 155-164, 2001.

[42] Ip, W.-H., A. Kopp, and J.-H. Hu, On the star-magnetosphhere interaction of close-in exoplanets, Astrophys. J., 602, L53-L56, 2004.

[43] Kaiser, M. L., P. Zarka, W. S. Kurth, G. B. Hospodarsky, and D. A. Gurnett, Cassini and Wind stereoscopic observations of Jovian nonthermal radio emissions : measurements of beamwidths, J. Geophys. Res., 105, 16053-16062, 2000.

[44] Kassim, N. E., R. A. Perley, W. C. Erickson, and K. S. Dwarakanath, Sub-arcminute resolution imaging of radio sources at 74MHz with the very large array, Astron. J., 106, 2218–2228, 1993.

[45] Kassim, N.E., T. J. W. Lazio, P. S. Ray, P. C. Crane, B. C. Hicks, K. P. Stewart, A. S. Cohen, and W. M. Lane, The low-frequency array (LOFAR): opening a new window on the universe, Planet. Space Sci., 52, 1343-1349, 2004.

[46] Khurana, K. K., M. G. Kivelson, D. J. Stevenson, G. Schubert, C. T. Russell, R. J. Walker, and C. Polanskey, Induced magnetic fields as evidence for subsurface oceans in Europa and Callisto, Nature, 395, 777-780, 1998.

[47] Kivelson, M. G., K. K. Khurana, C. T. Russell, R. J. Walker, J. Warnecke, F. V. Coroniti, C. Polanskey, D. J. Southwood, and G. Schubert, Discovery of Ganymede's magnetic field by the Galileo spacecraft, Nature, 384, 537-541, 1996.

[48] Kivelson, M. G., K. K. Khurana, F. V. Coroniti, S. Joy, C. T. Russell, R. J. Walker, J. Warnecke, L. Bennett, and C. Polanskey, The magnetic field and magnetosphere of Ganymede, Geophys. Res. Lett., 24, 2155-2158, 1997a.

[49] Kivelson, M. G., K. K. Khurana, C. T. Russell, R. J. Walker, P. J. Coleman, F. V. Coroniti, J. Green, S. Joy, R. L. McPherron, C. Polanskey, D. J. Southwood, L. Bennett, J. Warnecke, and D. E. Huddleston, Galileo at Jupiter - Changing states of the magnetosphere and first looks at Io and Ganymede, Adv. Space Res., 20, 193-204, 1997b.

[50] Kivelson, M. G., F. Bagenal, W. S. Kurth, F. M. Neubauer, C. Paranicas, and J. Saur, Magnetospheric interactions with satellites, in Jupiter: The Planet, Satellites, and Magnetosphere, edited by F. Bagenal, W. McKinnon, and T. Dowling, Cambridge University Press, Chapter 21, pp. 513-536, 2004.

[51] Knight, S., Parallel electric fields, Planet. Space Sci., 21, 741-750, 1973.

[52] Konovalenko, A. A., Ukraine decameter wave radioastronomy systems and their perspectives, in Radio Astronomy at Long Wavelengths, edited by R. G. Stone, K. W. Weiler, M. L. Goldstein, and J.-L. Bougeret, Geophysical Monograph 119. AGU, Washington, DC, pp. 311-319, 2000.

[53] Kraus, J. D., *Radio Astronomy*, Cygnus-Quasar Books, Powell, Ohio, 2^{nd} edition, 1986.

[54] Kurth,W.S., Gurnett, D.A., and Scarf, F.L., Control of Saturn's kilometric radiation by Dione, Nature 292, 742–745, 1981.

[55] Kurth, W. S., D. A. Gurnett, and J. D. Menietti, The influence of the Galilean satellites on radio emissions from the Jovian system, in Radio Astronomy at Long Wavelengths, edited by R. G. Stone, K. W. Weiler, M. L. Goldstein, and J.-L. Bougeret, Geophysical Monograph 119. AGU, Washington, DC, pp. 213-225, 2000.

[56] Lazio, T. J. W., W. M. Farrell, J. Dietrick, E. Greenlees, E. Hogan, C. Jones, and L. A. Hennig, The Radiometric Bode's Law and Extrasolar Planets, Astrophys. J., 612, 511-518, 2004.

[57] Lecacheux, A., A. A. Konovalenko, and H. O. Rucker, Using large radio telescopes at decametre wavelengths, Planet. Space Sci., 52, 1357–1374, 2004.

[58] Le Quéau, D., R. Pellat, and A. Roux, The Maser synchrotron instability in an inhomogeneous medium: Application to the generation of auroral kilometric radiation, Ann. Geophys., 3, 273-292, 1985.

[59] Louarn, P., Auroral planetary radio emissions: theoretical aspects, *Adv. Space Res.*, **12**, (8)121-(8)134, 1992.

[60] Menietti, J. D., D. A. Gurnett, W. S. Kurth, and J. B. Groene, Control of Jovian radio emission by Ganymede, Geophys. Res. Lett., 25, 4281-4284, 1998.

[61] Menietti, J. D., D. A. Gurnett, and I. Christopher, Control of Jovian radio emission by Callisto, Geophys. Res. Lett., 28, 3047-3050, 2001.

[62] Neubauer, F. M., Nonlinear standing Alfven wave current system at Io: Theory, J. Geophys. Res., 85, 1171-1178, 1980.

[63] Neubauer, F. M., The sub-Alfvénic interaction of the Galilean satellites with the Jovian magnetosphere, J. Geophys. Res., 103, 19843-19866, 1998.

[64] Prangé, R., L. Pallier, K. C. Hansen, R. Howard, A. Vourlidas, R. Courtin, and C. Parkinson, An interplanetary shock traced by planetary auroral storms from the Sun to Saturn, Nature, 432, 78-81, 2004.

[65] Prangé, R., D. Rego, D. Southwood, P. Zarka, S. Miller, and W. Ip, Rapid energy dissipation and variability of the Io-Jupiter electrodynamic circuit, Nature, 379, 323-325, 1996.

[66] Prangé, R., D. Rego, L. Pallier, J. E. P. Connerney, P. Zarka, and J. Queinnec, Detailed study of FUV Jovian auroral features with the post-COSTAR Hubble Faint Object Camera, J. Geophys. Res., 103, 20195-20215, 1998.

[67] Prangé, R., and P. Zarka, Planetary Aurorae, Invited paper #GAIII.14/07P/A12-007 at 23^{th} IUGG General Assembly, Sapporo, Japan, p. B-242, 29/6-11/7/2003.

[68] Preusse, S., A. Kopp, J. Büchner, and U. Motschmann, Stellar wind regimes of close-in extrasolar planets, Astron. Astrophys., 434, 1191-1200, 2005.

[69] Priest, E. R., The Sun and its magnetohydrodynamics, in Introduction to Space Physics, edited by M. G. Kivelson and C. T. Russell, Cambridge University Press, pp. 58-90, 1995.

[70] Queinnec, J., and P. Zarka, Flux, power, energy and polarization of Jovian S-bursts, Planet. Space Sci., 49, 365-376, 2001.

[71] Raterron, J.-M., Réalisation d'un Spectrographe Acousto-Optique: Analyse et traitement de l'information, Thèse de Doctorat, Observatoire de Paris-Meudon / Université Paris-Sud (XI), Orsay, 1985.

[72] Rubenstein, E. P., and B. E. Schaefer, Are superflares on solar analogues caused by extrasolar planets ?, Astrophys. J., 529, 1031-1033, 2000.

[73] Ryabov, V. B., P. Zarka, and B. P. Ryabov, Search of exoplanetary radio signals in the presence of strong interference : Enhancing sensitivity by data accumulation, Planet. Space Sci., 52, 1479-1491, 2004a.

[74] Ryabov, V. B., P. Zarka, and B. P. Ryabov, Detecting Radio-Bursts from Exoplanets: Instrumental and Statistical Limitations of Sensitivity in 1999-2001 Observations With UTR-2 Decameter Array, Proceedings of Joint AOGS 1st Annual Meeting & 2nd APHW Conference, p. 385, 2004b.

[75] Saar, S. H., Recent Measurements of Stellar Magnetic Fields, in Stellar surface structure, IAU Symp. 176, edited by K. G. Strassmeier and J. L. Linsky, Kluwer Academic Pub., Dordrecht, p. 237, 1996.

[76] Saar, S. H., and M. Cuntz, A search for Ca II emission enhancement in stars resulting from nearby giant planets, Mon. Not. R. Astron. Soc., 325, 55-59, 2001

[77] Saar, S. H., M. Cuntz, and E. Shkolnik, Stellar Activity Enhancement by Planets: Theory and Observations, in Stars as suns : activity, evolution and planets, IAU Symp. 219, edited by A. K. Dupree and A. O. Benz, Astronomical Society of the Pacific (ASP), San-Francisco, p. 355, 2004.

[78] Sanchez-Lavega, A., The magnetic field in giant extrasolar planets, Astrophys. J., 609, L87-L90, 2004.

[79] Saur, J., F. M. Neubauer, J. E. P. Connerney, P. Zarka, and M. G. Kivelson, Plasma interaction of Io with its plasma torus, in Jupiter: The Planet, Satellites, and Magnetosphere, edited by F. Bagenal, W.

McKinnon, and T. Dowling, Cambridge University Press, Chapter 22, pp. 537-560, 2004.

[80] Schaefer, B. E., King, J. R., and Deliyannis, C. P., Superflares on ordinary solar-type stars, Astrophys. J., 529, 1026-1030, 2000.

[81] Schneider, J., http://vo.obspm.fr/exoplanetes/encyclo/index.php, 2006.

[82] Shatten, K. H., Solar activity observations and predictions, edited by McIntosh and Dryer, MIT Press, Cambridge, 1972.

[83] Shkolnik, E., G. A. H. Walker, and D. A. Bohlender, Evidence for planet-induced chromospheric activity on HD 179949, Astrophys. J., 597, 1092-1096, 2003.

[84] Stevens, I. R., Magnetospheric radio emission from extrasolar giant planets: the role of the host stars, Mon. Not. R. Astron. Soc., 356, 1053-1063, 2005.

[85] Swarup, G., Giant metrewave radio telescope (GMRT) - Scientific objectives and design aspects, Indian Journal of Radio & Space Physics, 19, 493-505, 1990.

[86] Treumann, R.A. Planetary radio emission mechanisms: a tutorial, in Radio Astronomy at Long Wavelengths, edited by R. G. Stone, K. W. Weiler, M. L. Goldstein, and J.-L. Bougeret, Geophysical Monograph 119. AGU, Washington, DC, pp. 13–26, 2000.

[87] Van Haarlem, M. P. et al., LOFAR scientific applications, Report ASTRON-LOFAR-00230, v1.00, http://www.lofar.org, 2001.

[88] Vidal-Madjar, A., Lecavelier des Etangs, A., Désert, J.-M., G. E. Balester, R. Ferlet, G. Hébrard, and M. Mayor, An extended upper atmosphere around the extrasolar planet HD209458b, Nature, 422, 143-146, 2003.

[89] Willes, A. J., and K. Wu, Electron-cyclotron maser emission from white dwarf pairs and white dwarf planetary systems, MNRAS, 348, 285-296, 2004.

[90] Willes, A. J., and K. Wu, Radio emissions from terrestrial planets around white dwarfs, Astron. Astrophys., 432, 1091-1100, 2005.

[91] Winterhalter, D., G. Bryden, I. Chandra, W. Gonzalez, T. B. H. Kuiper, T. J. Lazio, W. Majid, R. A. Treumann, and P. Zarka, Search for radio emissions from extrasolar planets: the observation campaign, 6^{th} International Workshop on Planetary and Solar Radio Emissions (PRE VI), Graz, Austria, 20-22/4/2005.

[92] Zarka, P., The auroral radio emissions from planetary magnetospheres : What do we know, what don't we know, what do we learn from them ?, Adv. Space Res., 12, (8)99-(8)115, 1992.

[93] Zarka, P., Auroral radio emissions at the outer planets: observations and theories, J. Geophys. Res., 103, 20159-20194, 1998.

[94] Zarka, P., Radio emissions from the planets and their moons, in Radio Astronomy at Long Wavelengths, edited by R. G. Stone, K. W. Weiler, M. L. Goldstein, and J.-L. Bougeret, Geophysical Monograph 119. AGU, Washington, DC, pp. 167-178, 2000.

[95] Zarka, P., Nonthermal radio emissions from extrasolar planets, Extrasolar Planets: Today and Tomorrow, Astronomical Society of the Pacific (ASP), Vol. 321, edited by J.-P. Beaulieu, A. Lecavelier des Etangs and C. Terquem, San-Francisco, pp.160-169, 2004a.

[96] Zarka, P., Radio and plasma waves at the outer planets, Adv. Space Res., 33 (11), 2045-2060, 2004b.

[97] Zarka, P., Fast radio imaging of Jupiter's magnetosphere at low frequencies with LOFAR, Planet. Space Sci., 52, 1455-1467, 2004c.

[98] Zarka, P., Exoplanets and Solar System Science at Low Radio Frequencies, DGLR International Symposium To Moon and beyond, Bremen, Germany, 15-16/9/2005.

[99] Zarka, P., T. Farges, B. P. Ryabov, M. Abada-Simon, and L. Denis, A scenario for jovian S-bursts, Geophys. Res. Lett., 23, 125-128, 1996.

[100] Zarka, P., J. Queinnec, B. P. Ryabov, V. B. Ryabov, V. A. Shevchenko, A. V. Arkhipov, H. O. Rucker, L. Denis, A. Gerbault, P. Dierich, and C. Rosolen, Ground-Based High Sensitivity Radio Astronomy at Decameter Wavelengths, in Planetary Radio Emissions IV, edited by H. O. Rucker, S. J. Bauer, and A. Lecacheux, Austrian Acad. Sci. Press, Vienna, pp. 101-127, 1997.

[101] Zarka, P., R. A. Treumann, B. P. Ryabov, and V. B. Ryabov, Magnetically-driven planetary radio emissions and applications to extrasolar planets, Astrophys. Space Sci., 277, 293-300, 2001a.

[102] Zarka, P., J. Queinnec, and F. Crary, Low-frequency limit of Jovian radio emissions and implications on source locations and Io plasma wake, Planet. Space Sci., 49, 1137-1149, 2001b.

[103] Zarka, P., V. Ryabov, and B. Ryabov, Post-detection interference rejection and weak burst detection in time-frequency spectrograms, Proceedings of the URSI General Assembly, p2080, 2002.

[104] Zarka, P., B. Cecconi, and W. S. Kurth, Jupiter's low frequency radio spectrum from Cassini/RPWS absolute flux density measurements, J. Geophys. Res., 109, A09S15, doi:10.1029/2003JA010260, 2004.